Short-term variations in slip rate and size of prehistoric earthquakes during the past 2000 years on the northern San Jacinto fault zone, a major plate-boundary structure in southern California

Nathan W. Onderdonk[1,*], Sally F. McGill[2], and Thomas K. Rockwell[3]
[1]DEPARTMENT OF GEOLOGICAL SCIENCES, CALIFORNIA STATE UNIVERSITY–LONG BEACH, 1250 BELLFLOWER BOULEVARD, LONG BEACH, CALIFORNIA 90840, USA
[2]DEPARTMENT OF GEOLOGICAL SCIENCES, CALIFORNIA STATE UNIVERSITY–SAN BERNARDINO, 5500 UNIVERSITY PARKWAY, SAN BERNARDINO, CALIFORNIA 92407, USA
[3]DEPARTMENT OF GEOLOGICAL SCIENCES, SAN DIEGO STATE UNIVERSITY, 5500 CAMPANILE DRIVE, SAN DIEGO, CALIFORNIA 92182, USA

ABSTRACT

Most of the displacement across the North American–Pacific plate boundary in southern California is accommodated by the San Jacinto and the southern San Andreas fault zones. If and how the rate of displacement across these fault zones varies along strike and through time are still being resolved. Here, we present four calculations of late Holocene slip rate and average slip per event from the Claremont fault of the northern San Jacinto fault zone that show variations in strain distribution over the past 2000 yr and illustrate how plate-boundary displacement is distributed between the San Jacinto and southern San Andreas fault zones. We calculate a slip rate of 12.8–18.3 mm/yr and an average slip per event of 2.5 m from two measurements of streams offset by 9–11 earthquakes in the past 1500–2000 yr. Faster slip rates of 21–30 mm/yr and an average slip per event of 2.7–3 m were determined from measurements of a stream and a buried channel that were offset by three earthquakes in the past 400–500 yr.

The 2000 yr slip rate is similar to the range in slip rates reported for the adjacent San Bernardino section of the San Andreas fault zone, suggesting that the northern San Jacinto accommodates a similar amount of displacement as the San Andreas fault zone at the same latitude. The rate is also slightly faster (by ~2–3 mm/yr) than reported slip rates from the central San Jacinto fault zone to the southeast. A slip rate of 15 ± 2 mm/yr is within the range of uncertainty for almost all the geologic and geodetic data for the entire length of the San Jacinto fault zone and may be the best approximation for long-term average slip rate of the fault zone. Alternatively, 2–3 mm/yr of slip along the northern San Jacinto fault zone may be accommodated to the south along the lesser-studied Hot Springs, Thomas Mountain, Buck Ridge, and Santa Rosa faults, the lateral slip rates of which are not well known nor included in typical estimates of slip rate along the central San Jacinto fault zone.

We infer that the faster slip rate over the past 500 yr is due to a cluster of earthquakes along the Claremont fault between A.D. 1400 and A.D. 1850 and larger-than-average surface displacement of 3 m or more during the third event back. The 3 m or more measurement of displacement in this event corresponds to rupture lengths that are slightly longer than the total length of the Claremont fault, and previously published paleoseismic data indicate that this event occurred coincident in time with an event on the adjacent Clark fault. We propose that this combination of slip per event data and paleoseismic data from adjacent fault strands is strong evidence for rupture through the releasing step over that separates these two segments of the San Jacinto fault zone.

LITHOSPHERE doi:10.1130/L393.1

INTRODUCTION

Plate boundaries in continental crust typically consist of multiple fault zones. Although the far-field strain rates across these plate boundaries may be constant over hundreds of thousands to millions of years, the distribution of strain between the faults that make up the boundary can vary through time and along strike of the boundary (e.g., Atwater and Stock, 1998; Allen et al., 2004; Bennett et al., 2004). How this strain is distributed influences not only the tectonic evolution of the boundary, but also estimates of seismic hazard for local populations. This is especially important in southern California, where over 22 million people live along the Pacific–North American plate boundary. The southern California fault system is an excellent place to study how plate-boundary strain is distributed among faults because it consists of multiple fault zones that have a growing number of studies documenting fault slip rates, fault structure, and the timing and size of earthquakes during the past 2000 yr or more.

Slip rate measurements on individual faults in southern California from geologic, geomorphic, and geodetic data show that 50%–70% of the total plate-boundary displacement (52 mm/yr; DeMets and Dixon, 1999) is accommodated by the southern San Andreas fault zone and the San Jacinto fault zone combined (Fig. 1; e.g., Sharp, 1981; Weldon and Sieh, 1985; Morton and Matti, 1993; Spinler et al., 2010; McGill et al., 2013). However, the exact distribution of plate-boundary displacement between these two major faults is still unclear, and recent studies have suggested that slip rates may vary both along strike of the two faults zones (e.g., McGill et al., 2013; Blisniuk et al., 2010; Spinler et al., 2010) and through time (e.g., Sharp, 1981; Bennett et al., 2004) due to interaction with each other or nearby faults. Also unclear is whether surface ruptures along faults in these two zones

*nate.onderdonk@csulb.edu

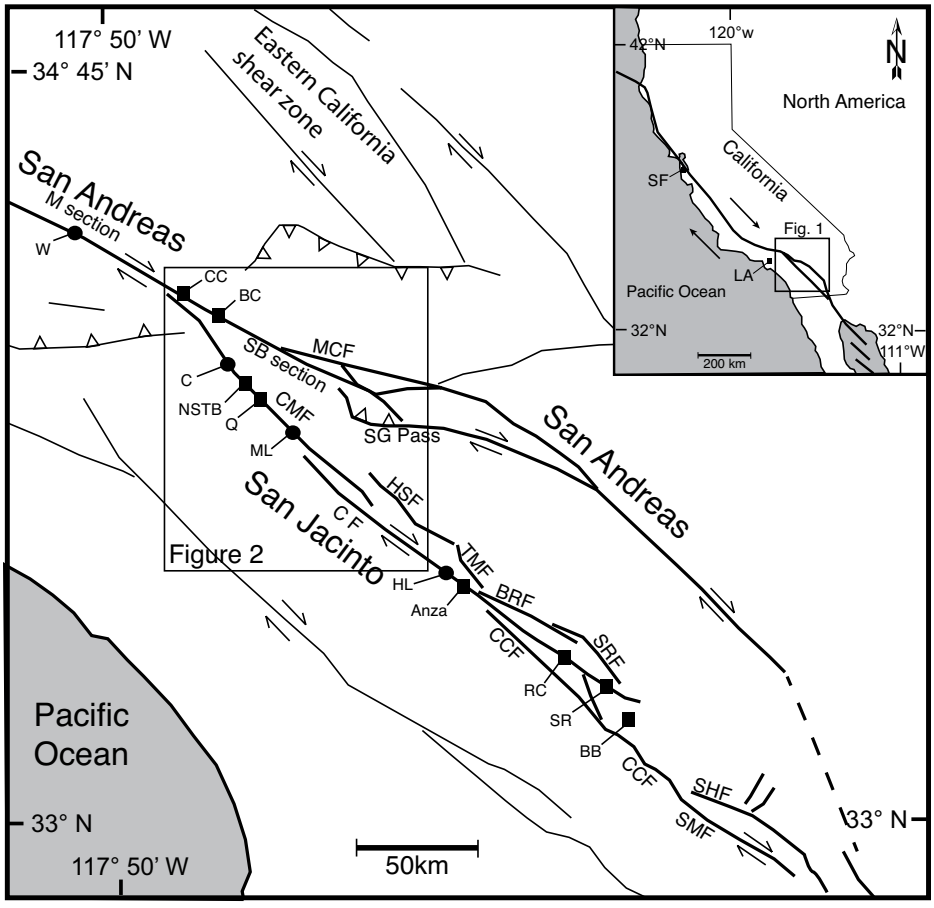

Figure 1. Map showing selected active faults in southern California. The southern San Andreas and San Jacinto fault zones are shown as bold lines, with major fault strands of the San Jacinto fault zone labeled (CMF—Claremont fault, CF—Clark fault, HSF—Hot Springs fault, TMF—Thomas Mountain fault, BRF—Buck Ridge fault, SRF—Santa Rosa fault, CCF—Coyote Creek fault, SHF—Superstition Hills fault, SMF—Superstition Mountain fault). Sections of the southern San Andreas fault that are pertinent to this study are also labeled (M section—Mojave section, SB section—San Bernardino section, SG Pass—San Gorgonio Pass fault zone, MCF—Mill Creek fault). Paleoseismic sites (black circles) and slip rate sites (black squares) include (from north to south) Wrightwood (W), Cajon Creek (CC), and Badger Canyon (BC) on the San Andreas fault zone, and Colton (C), northern San Timoteo Badlands (NSTB), Quincy (Q), Mystic Lake (ML), Hog Lake (HL), Anza, Rockhouse Canyon (RC), Santa Rosa (SR), and Borrego Badlands (BB) on the San Jacinto fault zone. Smaller inset map shows the location relative to the rest of California and the San Andreas fault (bold line); SF—San Francisco, LA—Los Angeles.

are related, and if so, how. For example, can rupture on the northern San Jacinto fault continue northward across the step over onto the San Andreas fault (Fig. 1), or trigger a separate rupture on the San Andreas fault? Or do the faults vary their coseismic displacement through time in antirelated earthquake clusters and lulls, as has been suggested for other parts of the fault system based on the timing of ruptures (Dolan et al., 2007).

We address these questions in this paper using new slip rate and slip per event data from the northern San Jacinto fault zone. Four new slip rate measurements refine the estimates of slip distribution between the San Bernardino segment of the San Andreas fault zone and the northern San Jacinto fault zone. The different time intervals over which the slip rates are calculated allow us to document variations in slip rate on the northern San Jacinto fault zone during the past 2000 yr. We also show how slip per event data can be used in conjunction with paleoseismic data from adjacent fault segments to infer rupture across step overs in a fault system.

BACKGROUND

Distribution of Plate-Boundary Slip across the Southern San Andreas Fault System

Differences in geologic measurements of slip rate along strike of the San Andreas fault in southern California indicate that some of the slip on the Mojave segment of the San Andreas fault is transferred to the northern San Jacinto fault zone (McGill et al., 2013; Morton and Matti, 1993; Weldon and Sieh, 1985). Slip rate measurements from the Mojave segment of the San Andreas fault average around 35 mm/yr (Matmon et al., 2005; Humphreys and Weldon, 1994; Salyards et al., 1992), whereas geologic slip rate measurements on the San Andreas fault from locations south of the juncture of the San Jacinto and San Andreas faults are 25 mm/yr at the most, and possibly as slow as 7 mm/yr along some fault segments in the San Bernardino and San Gorgonio Pass areas (Fig. 1; McGill et al., 2013; Behr et al., 2010; Yule and Spotila, 2010; Yule, 2009; Orozco, 2004; McGill et al., 2002, 2010; Harden and Matti, 1989; Weldon and Sieh, 1985).

Reported geologic slip rates from the Clark and Coyote Creek faults of the central and southern San Jacinto fault zone are mostly in the range of 10–15 mm/yr (Table 1), which agrees with slip rates of 12–15 mm/yr determined by most geodetic studies (Spinler et al., 2010; Becker et al., 2005; Fay and Humphreys, 2005; Meade and Hager, 2005). Bennett et al. (2004) inferred that slip rates on the San Jacinto fault zone have varied inversely with the southern San Andreas fault since the inception of the San Jacinto fault around 1.5 Ma (Morton and Matti, 1993; Janecke et al., 2011) based on apparent discrepancies in geologic slip rates determined over different time intervals. However, new dating and slip rate calculations led Blisniuk et al. (2013) to conclude that there was no observable change in slip rate through time on the central San Jacinto fault zone, at least for the past 0.5 m.y.

Previous slip rate measurements on the northern San Jacinto fault zone vary from less than 5 mm/yr to more than 25 mm/yr, and there are no measurements of total slip rate for time periods less than 35 k.y. (Table 1). Based on the southward decrease in slip rate on the San Andreas fault across the intersection with the San Jacinto fault zone, McGill et al. (2013) inferred that at least 12 mm/yr and possibly as much as 29 mm/yr of slip on the Mojave section of the San Andreas fault is transferred to the northern San Jacinto fault zone. This is a wide range, and if anything other than the minimum end of this range is correct, it would imply that the San Jacinto fault is currently accommodating more plate-boundary displacement than the southern San Andreas fault in the San Bernardino area. This idea, and the possibility of slip rate variation through time, cannot be tested with previously published geologic slip rate measurements on the northern San Jacinto fault because the calculated rates vary greatly, and

TABLE 1. PUBLISHED SLIP RATES FOR THE SAN JACINTO FAULT ZONE (SEE FIG. 1 FOR LOCATIONS)

Location (north to south)	Rate (mm/yr)	Age of offset feature(s)*	Dating method	Notes	Reference
Claremont fault					
Colton	~1.7–3.2	Ca. 1.9 ka	Radiocarbon	a	Wesnousky et al. (1991)
San Timoteo Badlands	6–13	50–100 ka	Soils		Prentice et al. (1986)
San Timoteo Badlands	8–20	50–100 ka	Soils		Morton and Matti (1993)
San Timoteo Badlands	16–20	1.5 Ma	Fossils	c	Morton and Matti (1993)
San Timoteo Badlands	>25	300–700 ka	OSL, soils	b	Kendrick et al. (2002)
San Timoteo Badlands	5–25 (**10–16**)	35.4–100 ka	^{10}Be, soils		McGill et al. (2011)
Clark fault					
Anza	~8–12	9.5 ka, 14 ka	Bishop Ash†	a	Sharp (1981)
Anza	6–23 (**10–14**)	17 ka, 50 ka	Soils		Rockwell et al. (1990)
Anza	10–15	4–4.8 ka	Radiocarbon		Merifield et al. (1991)
Anza	9.5–15.5	4.5 ka, 45 ka, 700 ka	^{26}Al and ^{10}Be		Blisniuk et al. (2013)
Rockhouse Canyon	6.9–10.9	28 ka, 47 ka	^{10}Be	d	Blisniuk et al. (2010)
Southern Santa Rosa Mtns.	1.1–1.9	35.7 ka	^{10}Be	d	Blisniuk et al. (2010)
Coyote Creek fault					
Coyote Creek	7–13	500–700 ka	Bishop Ash†		Dorsey (2002)
Southern San Jacinto fault					
Clark and Coyote Creek faults in Borrego Badlands	10.3–26.5	1.1 Ma	Paleomagnetism, sedimentological interpretations		Janecke et al. (2011)

Notes: **Bold** lettering indicates preferred values of a larger range. a—minimum rate because study did not assess all fault strands or due to stratigraphic interpretations; b—based on modeled lateral slip rates needed to match uplift rates of dated surfaces in a restraining bend, and ages shown are for uplifted deposits; c—based on inferred age of fault and total offset of bedrock deposits; d—lower rates southward on the Clark fault are due to partitioning of slip between the Clark and Coyote Creek faults. OSL—optically stimulated luminescence.

*Multiple ages mean multiple features of different ages were used to calculate slip rates.

†These studies used the presence of the Bishop Ash (758 ± 1.8 ka; Sarna-Wojcicki et al., 2000) to infer the approximate age of the sediments that contain it or lie stratigraphically above the ash.

most are based on displacement of tentatively dated deposits or do not directly measure displacement across the entire fault zone (Table 1). In this paper, we present new slip rate data from a site on the Claremont fault, which we call the Quincy site, that help to refine the large range in previously published rates.

Ruptures across Discontinuities in a Fault System

The San Jacinto fault zone consists of at least eight major fault strands that are separated by step overs (Fig. 1). Therefore, the rupture length and associated magnitude of earthquakes that can be generated in the San Jacinto fault zone depend on whether or not ruptures can continue across these steps. A releasing step over is also present between the northern end of the San Jacinto fault zone and the San Andreas fault zone (Figs. 1 and 2), which may or may not inhibit ruptures from propagating from one fault to the other. Similar timing of some prehistoric earthquakes on the Claremont fault and the Clark fault during the past 2000 yr led Onderdonk et al. (2013, 2014) and Rockwell et al. (2014) to infer that some ruptures may have propagated through the releasing step over that separates these two strands of the San Jacinto fault zone. They also noted similar timing of earthquakes on the Claremont fault and the Mojave segment of the San Andreas fault zone, suggesting the possibility that ruptures propagated from the northern San Jacinto fault zone to the San Andreas fault zone, or vice versa (Onderdonk et al., 2013, 2014; Rockwell et al., 2014). However, these interpretations are limited by uncertainties in the radiocarbon dates and stratigraphic relationships used to bracket the timing of the earthquakes, which can rarely be constrained to less than a decade, and are typically only constrained to several decades to a century. It is therefore impossible to know if two earthquakes documented at a similar time on adjacent faults are the same rupture, or different ruptures that occurred months, years, or even decades apart. However, combining overlaps in earthquake timing on two adjacent faults with interpretations of rupture length from slip per event data for specific earthquakes (Biasi and Weldon, 2006) can result in more confident interpretations regarding possible correlations of events. In this paper, we illustrate how this can be done using slip per event data from the Quincy site on the Claremont fault.

METHODS

The Quincy site was identified during field mapping of the Claremont fault (Figs. 2 and 3) and was chosen for further work based on the presence of deflected or offset streams and paleochannels. We use the term "paleochannel" to refer to stream channels that were offset by fault movement and then abandoned by avulsion and incision of a new channel across the fault. The site was mapped in the field on digital elevation model (DEM) base maps produced from the B4 light detection and ranging (LiDAR) point-cloud data set (Bevis et al., 2006) at a resolution of 0.5 m. Because there is only sparse vegetation in the field area, we did not filter out these aspects of the point cloud. Field mapping revealed several fault strands, three of which were inferred to be the main active strands that have deflected or offset numerous streams and resulted in abandoned paleochannels in some locations (faults A, B, and C, Fig. 3).

To measure the slip rate across these faults, we investigated two paleochannels associated with active drainages that are displaced by the faults. Our goal at both of these locations was to infer the inception age of the active drainages by dating the abandonment of the associated paleochannels, and then use the amount of displacement of the active drainages to calculate a slip rate. The timing of abandonment was determined at both locations by excavating trenches across the paleochannels and identifying and dating the upward transition from streamflow deposits to locally derived slopewash deposits exposed in these trenches (T1, T4, T5, T9, Fig. 3). Displacement of the active drainages was measured first on a computer using a DEM produced from the unfiltered LiDAR point cloud, and then in the field using a tape measure, along with LiDAR imagery to aid in identification of channel features. Maximum and minimum displacement amounts were measured parallel to the fault using the top edge of the offset stream channel walls as piercing points. We found that offset measurements can be refined in most places by field observations of the geology or geomorphology that are not visible in the LiDAR data, so we relied on our field measurements of displacement rather than those done on the computer. For example, at paleochannel 1 (Fig. 3), the exact upper edge of the channel walls was more difficult to define in the LiDAR data (including the use of cross sections through the topography) than in the field due to the resolution of the data and the presence of brush in one location. Filtering out the vegetation in the LiDAR point cloud did not increase the accuracy of the resultant DEM because the individual bushes were not very tall and are relatively dense. At paleochannel 2 (Fig. 3), outcrops of recent stream gravels were exposed in the walls of the active channel and indicated that recent incision had masked some of the total offset of the channel. This affected our interpretations of maximum and minimum

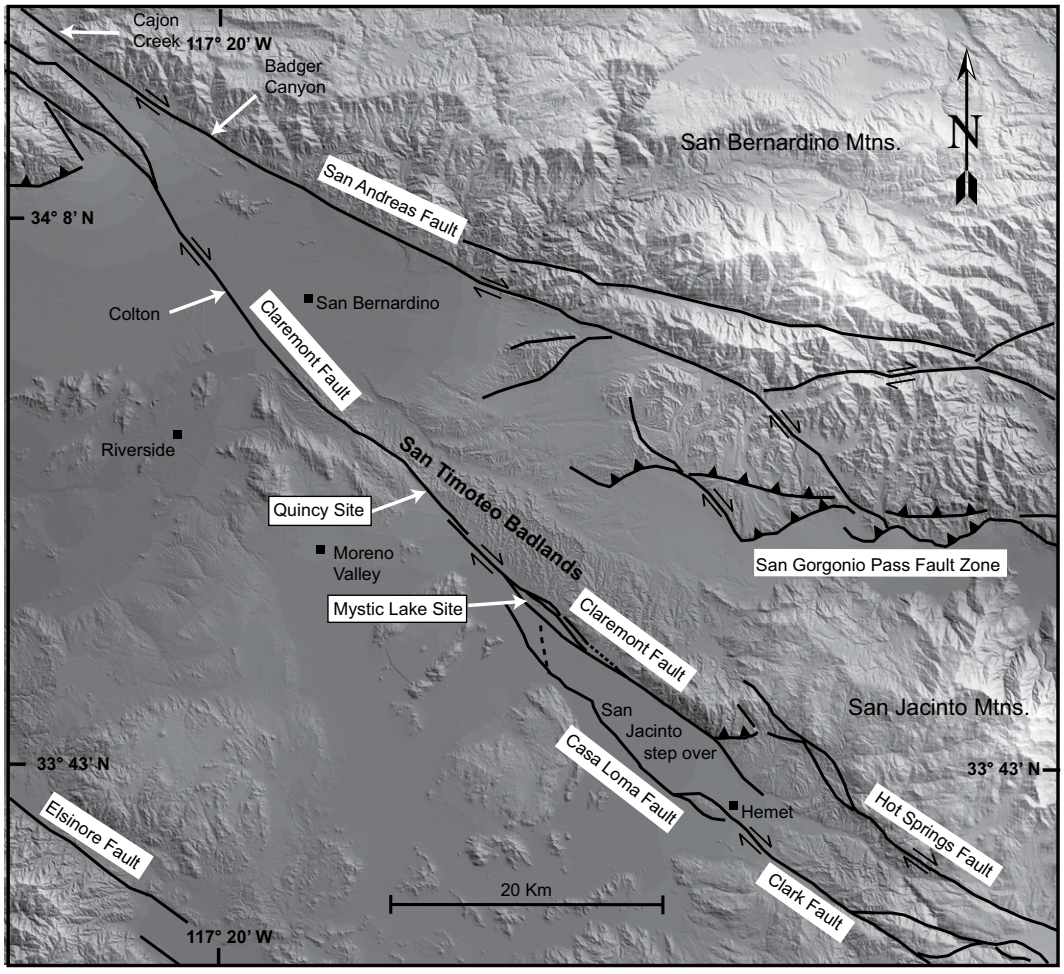

Figure 2. Hillshade image of a 30 m digital elevation model with the northern San Jacinto fault zone, San Bernardino section of the San Andreas fault zone, and the San Gorgonio Pass fault zone shown in black. Selected slip rate and paleoseismic sites are also shown. The cities of San Bernardino, Riverside, Moreno Valley, and Hemet are shown for reference.

offset amounts, and these relationships would not have been recognized in the LiDAR data alone. Based on our work at the Quincy site and other locations along the Claremont fault, we believe LiDAR data can greatly aid geomorphic interpretations needed to determine offset, but they should not replace field observations when precise measurements are needed.

Two other trenches were excavated across the faults in younger Quaternary deposits to search for evidence of recent ground-rupturing earthquakes (T2, T6, Fig. 3). In both of these trenches, we found evidence for the two most recent ruptures on the Claremont fault. Trench 6 also exposed a buried channel that was offset by faulting, so trenches 7 and 8 were excavated to trace the upstream continuation of the buried channel. Mapping of the offset buried channel in the trench walls, along with dating of the deposits and the faulting events, allowed us to measure the amount of offset along the faults and calculate a short-term slip rate and the average slip per event on the fault for the last two events.

Stratigraphic and structural relationships in every trench were logged in the field, and suitable detrital charcoal was collected for radiocarbon dating. We used a string grid to divide the walls into 1 m wide by 0.5 m tall panels, which were then photographed and annotated in the field. Detrital charcoal samples were dated at the Keck Carbon Cycle Accelerator Mass Spectrometry (AMS) Facility at University of California, Irvine, and were used to construct a stratigraphic model of the deposits in each trench. Stratigraphic models and radiocarbon dates were evaluated using OxCal (Bronk Ramsey, 2009) software to calibrate the radiocarbon dates and determine probability density functions for the age of deposits and the timing of avulsion events or earthquakes.

To calculate slip rates, we used the time between the earthquake prior to initiation of the active offset channel (or age of the buried channel) and the last (most recent) earthquake that displaced the channel, thereby capturing the time and amount of slip from complete earthquake cycles (Sieh and Jahns, 1984). A complete earthquake history for the past 2000 yr on the Claremont fault was documented from the Mystic Lake paleoseismic site (Onderdonk et al., 2013, 2014), which is located 11 km to the southeast of the Quincy site. We assumed that the earthquakes that ruptured through the Mystic Lake site also ruptured through the Quincy site and therefore used the timing of earthquakes at the Mystic Lake site to determine the amount of time over which the displacement of the offset features occurred. We also used the timing of earthquakes at the Mystic Lake site to calculate slip per event for the offset streams where there was no direct evidence at the Quincy site for the number or events that caused the displacement.

RESULTS

Fault Structure of the Quincy Site

Field mapping shows that there are three active fault strands that mark the topographic limit of the southwest margin of the San Timoteo Badlands (faults A, B, and C, Fig. 3). These are inferred to be the most active strands because of their location bounding the southwestern margin of the badlands and the presence of offset streams along their traces. Streams that cross

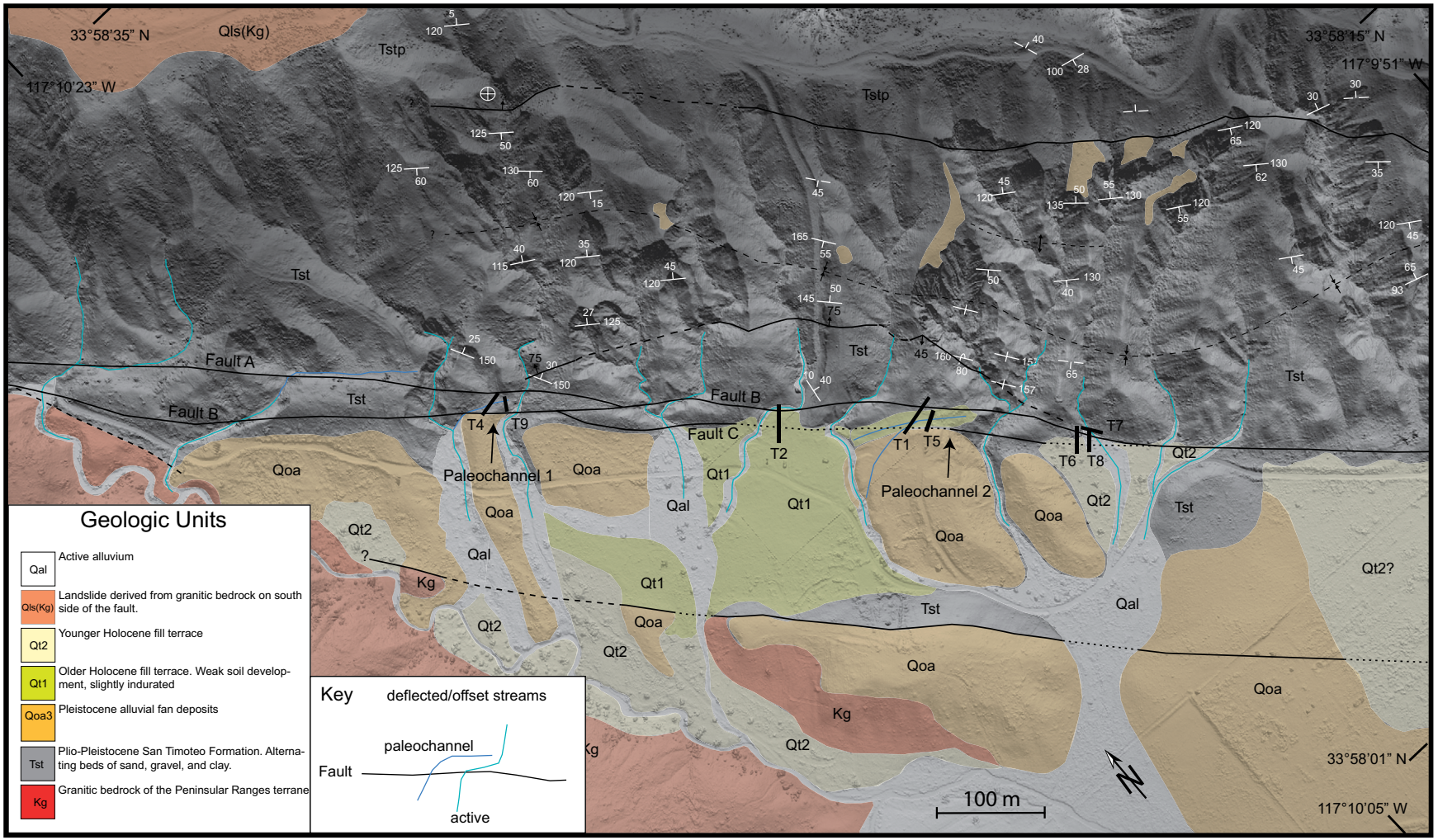

Figure 3. Geology, deflected and offset streams, trenches, and paleochannel study sites plotted on a 0.5 m resolution digital elevation model produced from the B4 light detection and ranging (LiDAR) data point cloud.

fault B are offset ~25 m to 30 m in a right-lateral sense and show evidence of recent incision in the form of oversteepened channel gradients upstream of the fault trace (Figs. 3 and 4). Fault A is located in the northwestern part of the site and has offset a stream by ~105 m, the fault-parallel section of which has been abandoned due to avulsion. Fault C is located at the front of the badlands and also marks an older offset and associated paleochannel that is between 65 and 85 m in length. Neither fault A nor C shows clear offset of the younger incised streams, and both are truncated by fault B. Where exposed in outcrops and trenches, all three faults dip nearly vertically or steeply to the northeast and are expressed as 0.25–2-m-wide zones of sheared and shattered rock with seams of clay gouge. Fault strands B and C merge into a single strand to the southeast, and strands A and B merge to the northwest of the site.

Two other fault strands are present at higher elevations to the northeast, both of which we infer to be older based on their lack of geomorphic expression. These older fault strands do not offset streams, are only faintly expressed in the geomorphology, and were mainly identified by geologic mapping and discontinuities in structure and stratigraphy identified in outcrops. A fifth fault strand is located ~80 m to the southwest of the badlands. It does not show strong geomorphic evidence of recent activity in this area, but it does show vertical displacement of the older Quaternary alluvium (Qoa, Fig. 3) along its southwest side. The well-developed soil on this alluvial deposit suggests that the deposit is at least a few tens of thousands of years in age, so the fault has moved in the late Pleistocene and possibly in the Holocene, but we were not able to determine the slip history of this strand. This fault appears to be the contact between the Quaternary San Timoteo Formation sedimentary rock on the northeast side of the fault and Mesozoic granitic and metamorphic rock on the southwest side of the fault and merges with the main active strands at the northwestern edge of the site.

Displacement Amount and Age of Offset Stream Channels

Trenches excavated across the two paleochannel sites and the buried channel site revealed stratigraphic relationships and detrital charcoal that allowed us to infer the age of the offset features. The amount of offset of the active channels at the

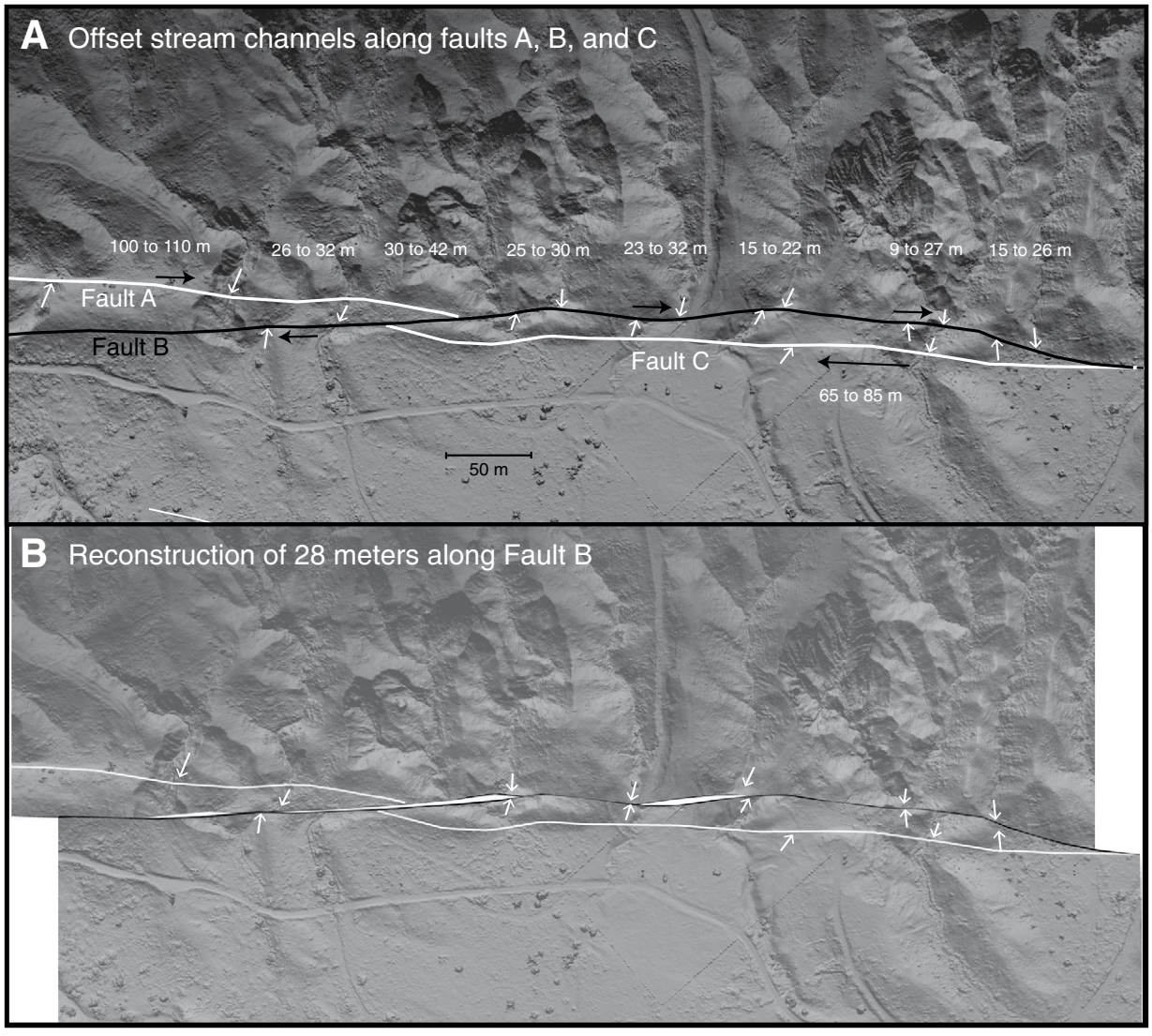

Figure 4. (A) Primary faults at the Quincy site are shown with arrows indicating correlative upstream and downstream channel piercing lines. Maximum and minimum displacement amounts of the stream offsets are shown in white above the offset streams. (B) Reconstruction of 28 m along fault B.

TABLE 2. SUMMARY OF OFFSET MEASUREMENTS, FEATURE AGE, NUMBER OF EVENTS THAT OFFSET THE FEATURES, TIME RANGE OVER WHICH THE OFFSET ACCRUED, AND CALCULATED SLIP RATE AND SLIP PER EVENT FOR EACH FEATURE AT THE QUINCY SITE

	Buried channel	Paleochannel 1		Paleochannel 2		Total offset on fault B
		NW	SE	NW	SE	
Offset						
Minimum	5.4 m	9 m	4.5 m	8.8 m	–	25 m
Maximum	5.9 m	18.9 m	9 m	27 m	–	42 m
Preferred	–	16.9 m	6.5 m	18–25 m		–
Preferred	**5.4–5.9 m**	**9 m**		**18–25 m**		**25–30 m**
Age of offset feature	A.D. 1521–A.D. 1648	A.D. 1426–A.D. 1494		A.D. 345–A.D. 520		167 B.C.–A.D. 70
Number of events*	2 or 3	3 or 4		9 or 10		**11**
Time range of accrued offset*	128–329 yr	300–428 yr		1230–1606 yr		1639–1953 yr
Slip rate						
Full range	16.4–46 mm/yr	6.7–63 mm/yr		5.5–22 mm/yr		12.8–25 mm/yr
Preferred†	**16.4–46 mm/yr**	**21–30 mm/yr**		**11.3–20.3 mm/yr**		**12.8–18.3 mm/yr**
Slip per event						
Full range	1.8–2.95 m	1.5–6.3 m		0.53–3 m		2.3–3.8 m
Preferred†	**2.7–2.95 m**	**3 m**		**1.8–2.8 m**		**2.3–2.7 m**

Notes: Offset features are listed youngest to oldest. Bold lettering indicates preferred numbers. NW and SE denote measurements of channel walls for paleochannels 1 and 2. Details of the slip rate calculations are presented in the Appendix.
*Inferred from the timing of events at the Mystic Lake site.
†Based on preferred offset amounts and preferred number of events.

two paleochannel sites was determined using the geomorphology of the channels. The amount of offset of the buried channel was determined by tracing the channel through the subsurface using multiple trenches and progressive excavation. The offset amounts and ages from each site are summarized in Table 2, and details are presented next from the northwest to the southeast (Fig. 3).

Paleochannel 1

Trench exposures. We excavated two trenches across paleochannel 1 (Fig. 5). Trench 4 was excavated first and exposed fault B at the southwestern end of the trench. The fault zone was expressed as a 1-m-wide zone of sheared San Timoteo Formation sedimentary sandstone and conglomerate with subvertical, 1–8 cm bands of clay gouge, surrounded by a 1.5–2-m-wide zone of shattered rock (Fig. 6). Approximately 2 m northeast of the main fault, younger unconsolidated sediments were exposed that were deposited unconformably on shattered and weathered San Timoteo Formation. The sediments in the deeper part of the trench (from 1.5 m below the surface to the bottom of the trench at 3 m depth) consisted of rounded cobbles, well-sorted sand, and well-sorted pebbles. We interpret these sediments to be channel deposits from streamflow when the paleochannel was active. The bottom of these channel deposits was not reached in trench 4 and must be greater than 3 m deep. However, both the northeast and southwest sides of the channel were exposed where the channel deposits were scoured into weathered sandstone, mudstone, and conglomerate of the San Timoteo Formation. Stratigraphically above these channel deposits, the trench exposed sediments composed of fine-grained silt, unsorted matrix-supported pebbles, and isolated sandy lenses. There was no evidence of significant streamflow, and we interpret these deposits to be slope wash derived from the slopes directly to the northeast of the paleochannel. The change from coarser, well-sorted channel deposits to unsorted silty slope-wash deposits is interpreted to mark the timing of avulsion and abandonment of the paleochannel (Fig. 6). At least two organic-rich layers were present within the transition zone between the deeper channel deposits and the overlying slope-wash deposits. We interpret these layers to be weak paleosols that represent soil development at the surface after the paleochannel was abandoned.

We excavated a second trench (trench 9) 15 m closer to the active channel to provide additional exposures and to see how the

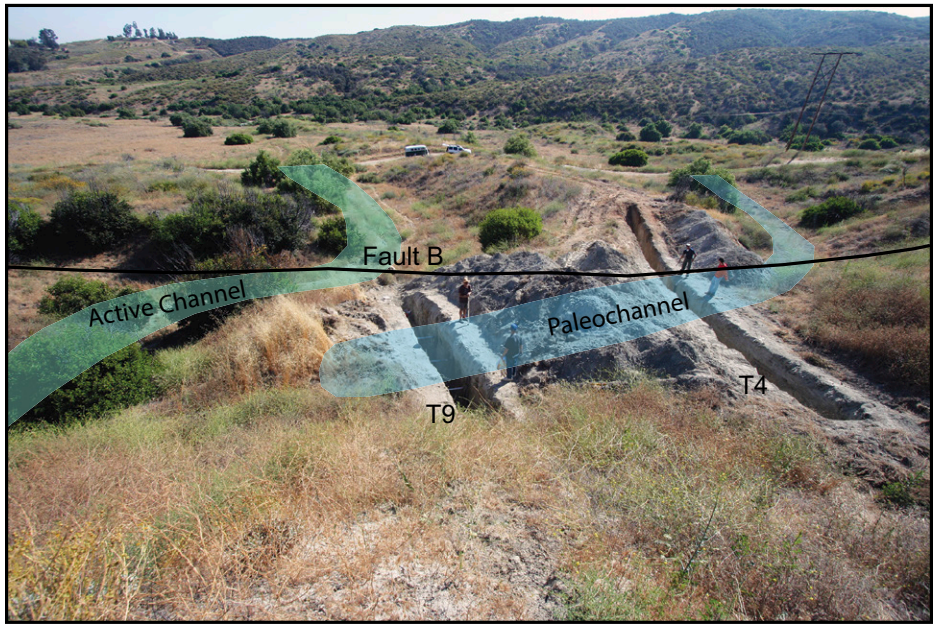

Figure 5. Photograph looking southwest across fault B at paleochannel 1. Blue shading indicates the location of the paleochannel based on surface morphology and exposure in trenches 9 and 4. Green shading indicates the location of the active channel.

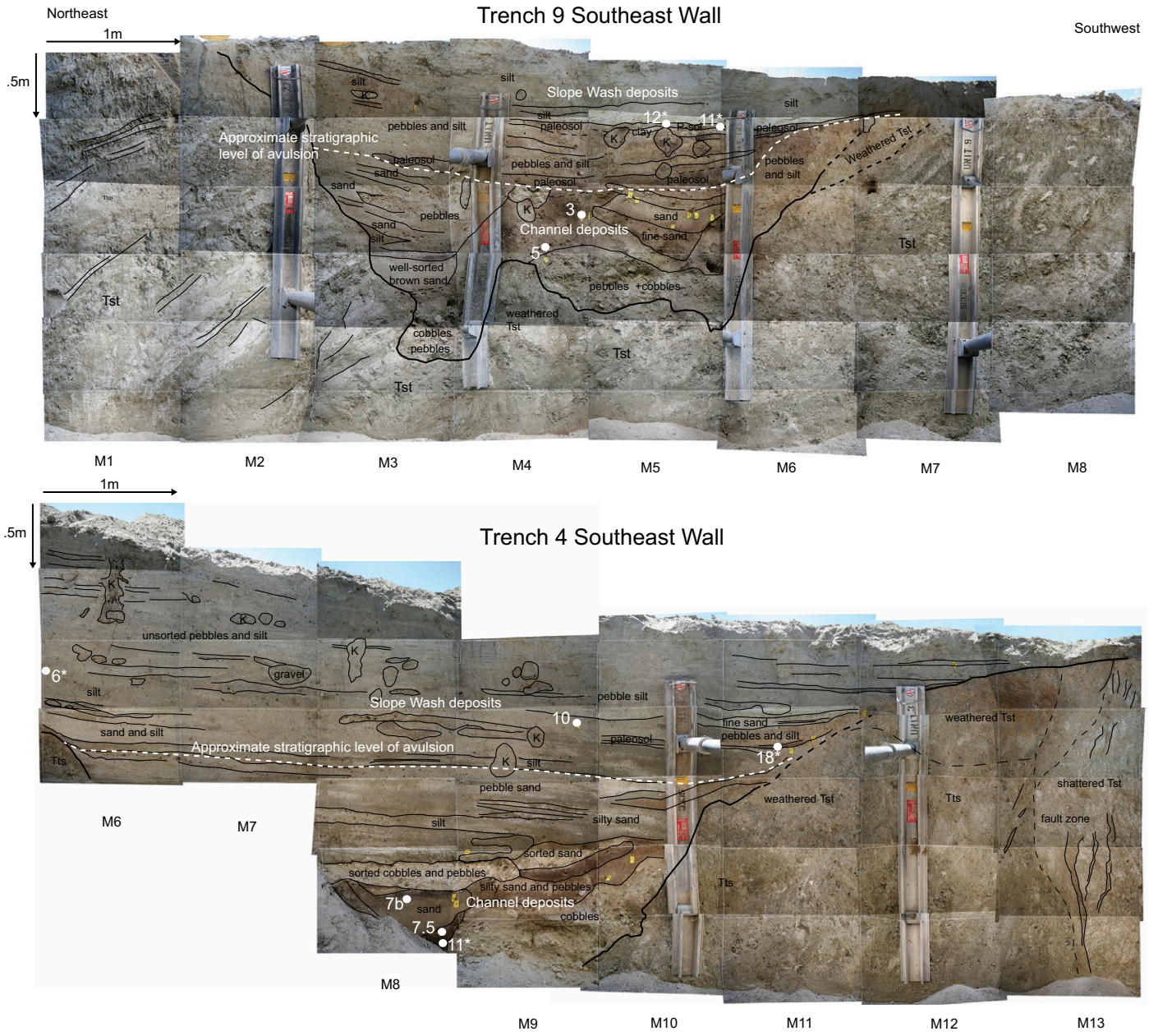

Figure 6. Photomosaics of the southeast walls of trench 9 and trench 4 showing stratigraphic relationships and locations of dated detrital charcoal samples (white dots with numbers; * indicates sample was collected from the opposite wall) used to infer the time of paleochannel avulsion and capture by the modern stream. Bold black line indicates the base of the paleochannel, and the white dashed line indicates the approximate stratigraphic level of the avulsion based on sedimentology and the presence of paleosols. Tst—Tertiary San Timoteo Formation and K—krotovina.

paleochannel changed in the upstream direction (Fig. 6). The base of the paleochannel was shallower (as would be expected upstream) and showed the same stratigraphic relationships as in trench 4. The upper meter of sediment consisted of poorly sorted pebbly silt overlying two paleosols. The two paleosols had formed on top of deposits of well-sorted sand, pebbles, and rounded cobbles that are present between 1 and 2 m depth. The bottom of the channel was exposed in trench 9 and was seen as an uneven surface scoured into the underlying San Timoteo Formation. Beds in the San Timoteo Formation dipped 30°–40° to the northeast in the trench walls. The main fault zone was not exposed in trench 9 because trench 9 was not excavated into the active channel where the main fault is located. As in trench 4, we interpret the avulsion event to be represented in the stratigraphy by the change in facies from channel deposits to slope-wash deposits, separated by the development of the two paleosols.

Timing of avulsion and initiation of the active channel. Detrital charcoal was present in both trenches and was collected and dated to determine the timing of the avulsion, which we infer to be the best indicator for the timing of the capture by the modern channel that has now been offset by continued fault activity. Radiocarbon dates (Table 3) were calibrated using OxCal (Bronk Ramsey, 2009), and age models were constructed for the individual trenches; these models were combined to produce a compos-

TABLE 3. DATED ^{14}C SAMPLES, QUINCY SITE, SAN JACINTO FAULT

Trench	Sample number	Age (^{14}C yr)	±	Calibrated age (yr, 2σ)	Area under PDF curve	Notes
Paleochannel 1						
4	10	130	15	1681–1710	0.17	After avulsion
				1717–1739	0.122	
				1750–1762	0.026	
				1802–1890	0.515	
				1909–1938	0.168	
9	11	275	40	1486–1604	0.553	After avulsion
				1607–1670	0.378	
				1780–1798	0.06	
				1944–1950	0.009	
9	12	295	15	1521–1576	0.669	After avulsion
				1584–1590	0.016	
				1625–1649	0.315	
4	6	310	35	1481–1651	1	After avulsion
4	18	385	15	1449–1511	0.864	After avulsion
				1601–1616	0.136	
4	*8*	*1900*	*100*	*B.C. 115–A.D. 348*	*0.984*	*Older than samples from same layer*
4	7b	470	15	1423–1446	1	Before avulsion
4	7.5	560	70	1286–1446	1	Before avulsion
4	11	635	15	1291–1320	0.386	Before avulsion
				1350–1391	0.614	
9	3	940	30	1026–1158	1	Before avulsion
9	5	1220	15	721–740	0.117	Before avulsion
				767–782	0.152	
				786–879	0.732	
4	*22*	*400*	*15*	*144–1491*	*0.975*	*Out of strat order. Bioturbated?*
				1603–1609	*0.025*	
Paleochannel 2						
1	7humus	1290	15	670–722	0.621	After avulsion
				740–767	0.379	
1	7a	1305	20	662–719	0.712	After avulsion
				742–766	0.288	
1	4	1600	20	406–476	0.476	After avulsion
				483–536	0.524	
1	*3*	*90*	*20*	*1694–1727*	*0.272*	*Out of strat order. Bioturbated?*
				1812–1919	0.728	
1	5	1680	20	265–273	0.023	Before avulsion
				331–412	0.977	
1	2	1945	20	6–88	0.937	Before avulsion
				102–121	0.063	
1	9humus	2145	180	B.C. 751–B.C. 682	0.027	Before avulsion
				B.C. 668–B.C. 636	0.011	
				B.C. 626–B.C. 614	0.003	
				B.C. 592–A.D. 237	0.958	
1	9a	2125	35	B.C. 350–B.C. 303	0.107	Before avulsion
				B.C. 210–B.C. 48	0.893	
1	6	23,850	100	Out of range		Older alluvium
				Trench 2		
2	2	895	20	1044–1099	0.431	Predates both events
				1119–1143	0.125	
				1146–1210	0.443	
2	4	230	20	1644–1670	0.573	Predates both events
				1779–1799	0.381	
				1943–1950	0.046	
2	25	190	15	1663–1682	0.228	Predates both events
				1737–1757	0.111	
				1761–1804	0.461	
				1936–1950	0.2	
2	31	2205	20	B.C. 360–B.C. 269	0.583	Strata covering fault A
				B.C. 264–B.C. 202	0.417	
2	*8*	*–1690*	*20*			*Modern carbon*
2	*23*	*3860*	*45*	*B.C. 2464–B.C. 2205*	*1*	*Older than sample from same unit*
Trenches 6 and 7						
6	6	135	15	1679–1707	0.169	Postdates E2, predates E1
				1719–1764	0.206	
				1800–1826	0.123	
				1832–1886	0.313	
				1912–1939	0.188	
6	3	235	15	1646–1667	0.697	Postdates E2, predates E1
				1783–1796	0.303	
6	11	300	15	1521–1578	0.698	Offset channel and predates events
				1582–1591	0.029	
				1622–1647	0.273	
7	1a	305	15	1520–1592	0.758	Offset channel age
				1619–1645	0.242	

Notes: Samples in italics were omitted from the OxCal models. All calibrated ages are A.D. unless labeled otherwise. PDF—probability density function.

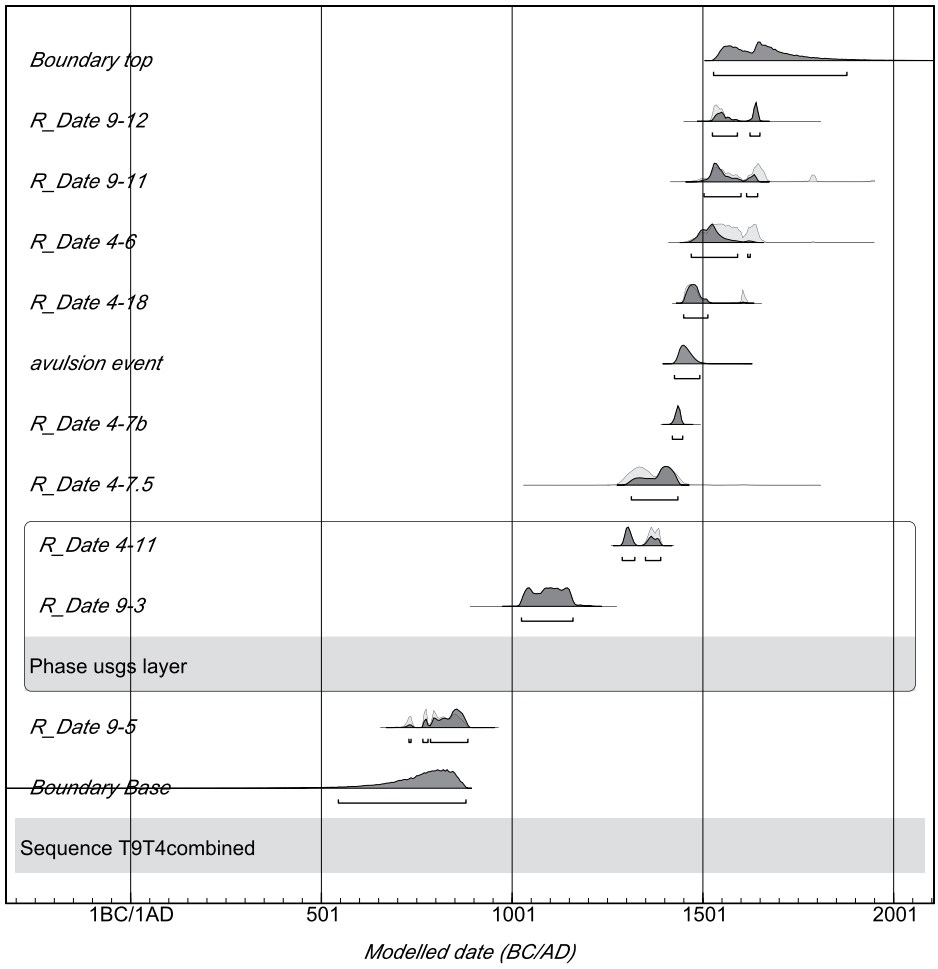

Figure 7. OxCal (Bronk Ramsey and Lee, 2013) model of the age of stratigraphic units in trenches 4 and 9 and the timing of the avulsion of paleochannel 1 to the modern channel.

ite model that used the data from both trenches (Fig. 7). The samples collected from the channel deposits below the stratigraphic level attributed to the avulsion span a time period of ~750 yr, from A.D. 700 to A.D. 1450. The four samples collected stratigraphically above the interpreted avulsion event span a time period of only 200 yr, from A.D. 1450 to A.D. 1650. Three of these four samples were collected from paleosols that probably formed shortly after the avulsion event, which we infer to be the cause of the tightly clustered ages. The ages of the samples collectively constrain the timing of the avulsion event to be between A.D. 1426 and A.D. 1494 (Fig. 7). We therefore infer that the active channel was initiated 519–587 yr B.P. (2014).

Displacement of the active channel. Displacement of the active channel was measured in the field using a tape measure. We measured the maximum, minimum, and preferred displacement amounts for both channel margins (Fig. 8). We interpret an apparent right-lateral offset of the channel by ~3–5 m along fault A to be the result of a landslide from the northwest canyon wall that has deflected the stream. Consequently, we infer that the offset along fault B represents the full amount of offset since capture and incision by the active channel. We used the top of the channel walls as piercing lines because we believe that the top angles should be more stable than the bottom of the channel edges, where incision, lateral stream erosion, and sediment deposition may modify the position of the base of the channel wall more rapidly and dramatically. The northwest channel wall was offset a minimum of 9 m and maximum of 18.9 m, with a preferred offset of 16.9 m. The southwest channel wall was offset a minimum of 4.5 m and a maximum of 9 m, with a preferred offset of 6.5 m.

We do not report uncertainties in the measurements themselves because we consider the uncertainty in the geomorphic interpretation to include (and far outweigh) the measurement uncertainty in the field. Our maximum and minimum measurements include any uncertainty

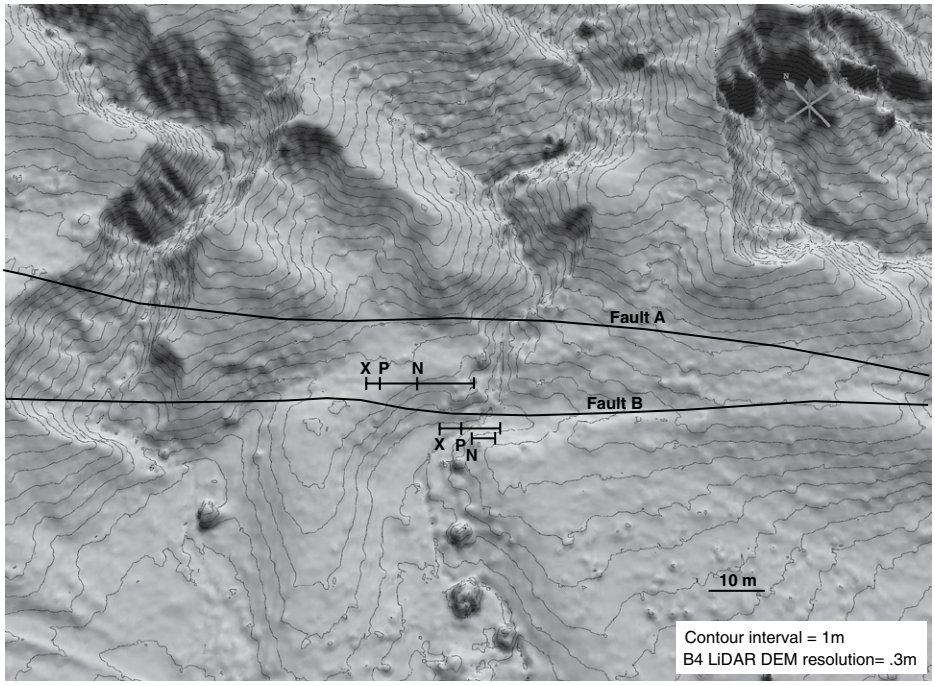

Figure 8. Faults and measurements of displacement of the northwest and southeast stream channel walls plotted on a 0.3-m-resolution digital elevation model (DEM) produced from light detection and ranging (LiDAR) data. Maximum (X), preferred (P), and minimum (N) amounts of displacement are shown.

associated with identifying the exact upper edge of the channel walls. The measurements from the southeast wall were consistently smaller than those from the northwest wall. This is likely due to erosion of the southeast wall as the southwest side of the fault has been displaced into the stream channel, causing the offsets to be smaller than the actual displacement along the fault. The alternative explanation is that the northwest channel wall on the downstream side of the fault (southwest side) has been eroded toward the northwest at the outside bend in the stream, producing a separation of the channel wall that is larger than the actual tectonic displacement. Some lateral erosion of one or both walls of the channel downstream of the fault must have occurred because the downstream segment is approximately twice as wide as the upstream segment, and it is likely that erosion of both channel walls on the downstream side of the fault has occurred. The displacement amounts from the two channel walls overlap around 9 m. The geomorphology indicates that the northwest channel wall was displaced at least 9 m, and that the southeast channel wall could not have been displaced more than ~9 m. We therefore use 9 m as our preferred amount of displacement.

Paleochannel 2

Trench exposures. Two trenches were excavated across paleochannel 2, but only trench 1 was evaluated in detail due to the higher degree of bioturbation and poorly defined stratigraphy in trench 5. Trench 1 exposed at least two nested fluvial channels in the deeper part of the trench (2–3 m depth) that consisted of poorly bedded sand, pebbles, and weathered clasts of San Timoteo coarse sandstone and pebble conglomerate (Fig. 9). An organic-rich layer capped the older of these channels, but it was cut by the stratigraphically higher channel. Overlying these channel deposits, there was 1 m of bedded sand, silty sand, and clay-rich silt with pebbles that we also interpret to be fluvial channel deposits. Two organic-rich paleosol layers separate these fluvial deposits from an overlying deposit of massive, bioturbated silt that is derived from the local slopes. As in trenches 4 and 9 at paleochannel 1, we infer that the weak paleosols (A horizons) that are present at the change in stratigraphy from fluvial deposits to slope-wash deposits represent weathering and soil formation after abandonment of the paleochannel. Hence, we interpret that the stratigraphic level of the avulsion event is directly under these paleosols.

Two faults were found to be present at 2–3 m depth, which corresponds with the position of fault C at the surface (Fig. 9). The older fault, fault 1, was expressed as a 2–3-cm-thick zone

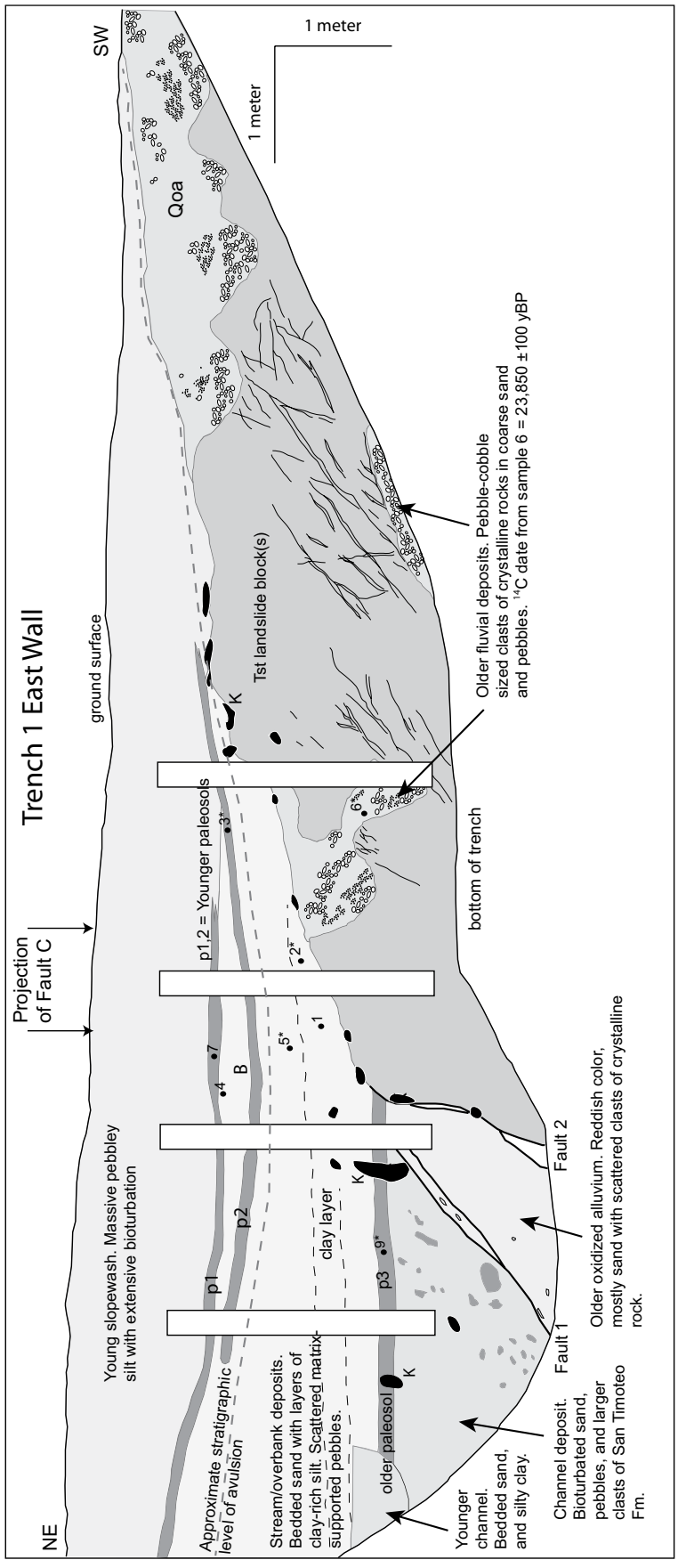

Figure 9. Stratigraphic relationships exposed in the east wall of trench 1 excavated across paleochannel 2. Dated detrital charcoal samples are shown as block dots with numbers (* indicates sample was collected from the opposite wall). Vertical white rectangles are areas hidden by trench shores. Approximate stratigraphic level of the avulsion is shown as a dashed black line. Photomosaic techniques were not used in this trench. Tst—Tertiary San Timoteo Formation, Qoa—Quaternary older alluvium, and K—krotovina.

of clay gouge and sheared rock that dipped 45° to the northeast. The fault separated well-sorted sand, pebbles, and some larger weathered clasts of San Timoteo Formation on the northeast from oxidized sand with clasts of granitic and metamorphic rocks on the southwest, and it was truncated upward by a dark organic-rich layer that we interpret to be a weak paleosol (A horizon). Fault 2 was also expressed as a thin zone of clay gouge that dipped 85° to the northeast and separated the oxidized sand and overlying paleosol from San Timoteo Formation on the southwest. The San Timoteo rock was found to be highly fractured and occurred in several large blocks, which we interpret to be large slide blocks separated by zones of bedded cobbles, pebbles, and sand that were locally tilted.

Timing of avulsion and initiation of the active channel. Detrital charcoal and bulk samples of the paleosols were collected and dated to estimate the timing of the avulsion and initiation of the active channel adjacent to the paleochannel (Table 3). Figure 10 shows the OxCal model for trench 1, and the dates indicate that the avulsion occurred sometime between A.D. 345 and A.D. 520. The dates from the deeper paleosol cut by fault 2, along with the dates from layers that cap fault 2, show that the most recent event on fault C occurred between 167 B.C. and A.D. 70. Consequently, we infer that all activity for the past two millennia has occurred on fault B. This most recent earthquake on fault C overlaps in time with event 12 at Mystic Lake (Fig. 11; Onderdonk et al., 2013).

Displacement of the active channel. Displacement of the active channel at this location is not as clearly expressed in the geomorphology as it is at other drainages in the area. The upstream and downstream segments of the active channel are displaced across the two faults (Fig. 12), but the bottom of the present thalweg and southeast channel wall do not show any clear fault-parallel segment and are instead oriented diagonally between the two faults. This geometry gives the impression that the channel experienced distributed shear in the zone between the two faults, but the lack of evidence in the trench exposures for shear or faulting between faults B and C makes this interpretation unlikely. We think the geometry is most likely due to recent incision that has eroded any fault-parallel segment that previously existed. Incision of this active channel relative to the paleochannel has been deeper than for most drainages in the area because of

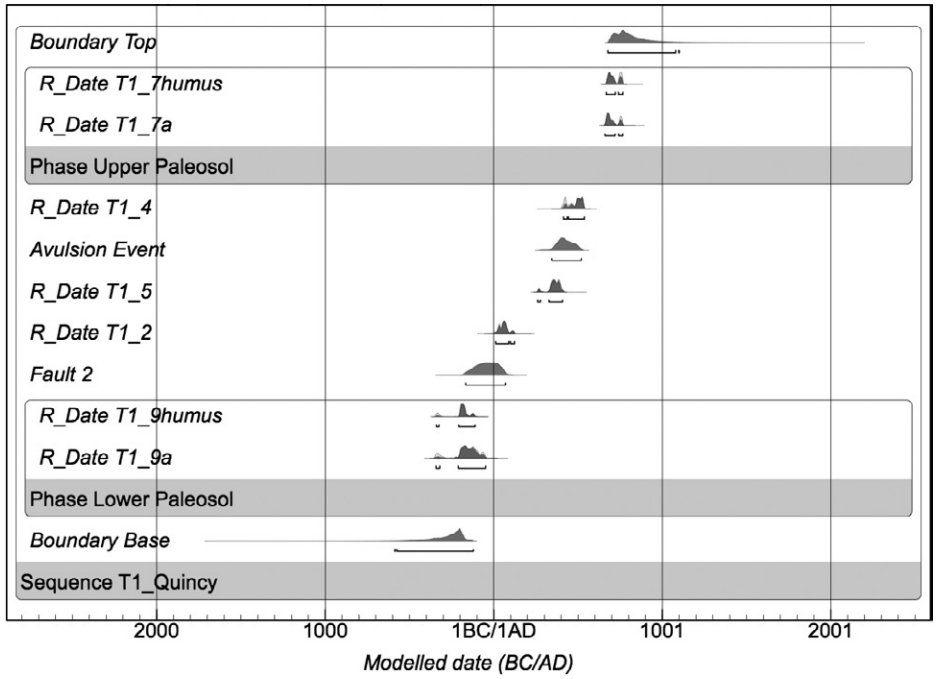

Figure 10. OxCal (Bronk Ramsey and Lee, 2013) model of the age of stratigraphic units in trench 1 and the timing of faults and the avulsion of paleochannel 2.

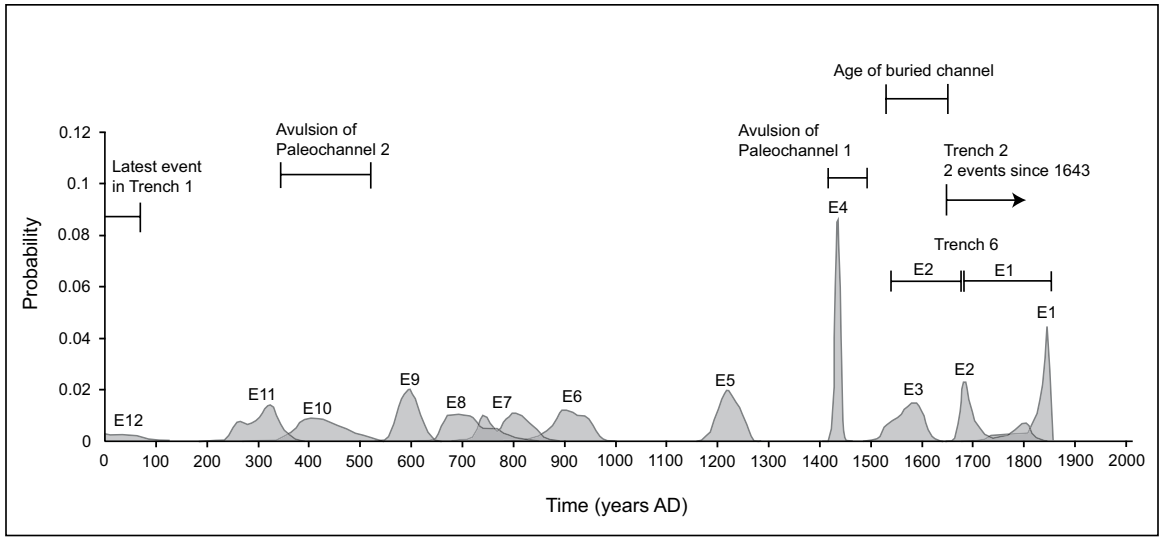

Figure 11. Probability density functions of the timing of events recorded at the Mystic Lake site. The ages of events and features used to calculate slip rate and slip per event at the Quincy site are plotted above, along with the timing of earthquakes recorded in trenches 1, 2, and 6.

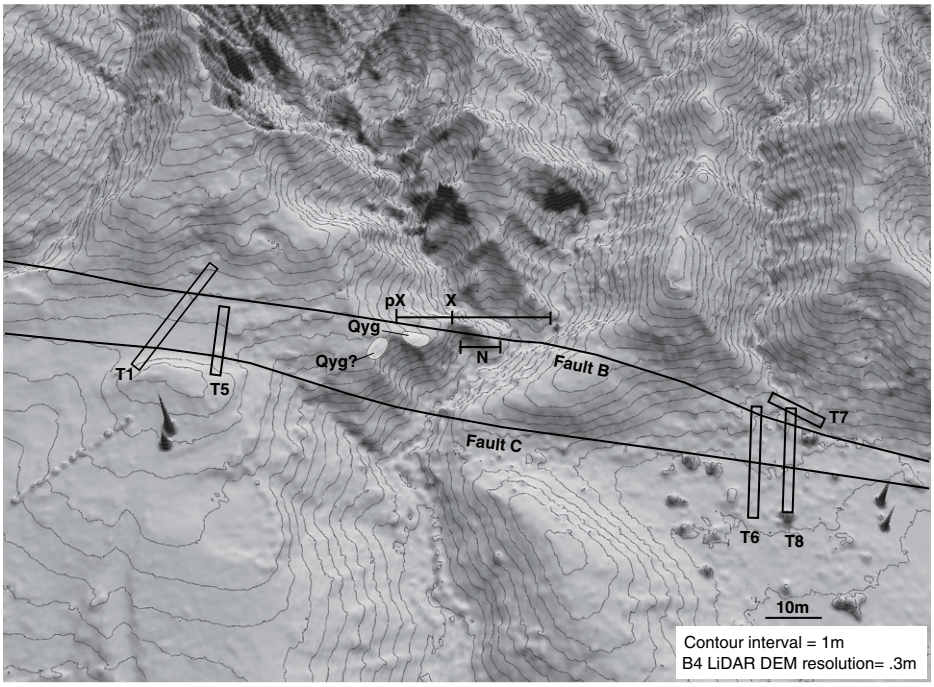

Figure 12. Faults, nearby trenches, and measurements of displacement of the northwest stream channel wall plotted on a 0.3-m-resolution digital elevation model (DEM) produced from light detection and ranging (LiDAR) data. Paleomaximum (pX) is the displacement if the Quaternary gravels (Qyg) exposed near the top of the northwest wall are from stream deposition prior to late incision of the stream. Maximum (X) and minimum (N) displacement of the present-day morphology are also shown.

the older alluvial deposits and elevated topography on the southwest side of the fault at this location. For example, the bottom of the active channel here is ~11 m below the elevation of paleochannel 2, whereas at paleochannel 1, the elevation difference between the channel bottom and paleochannel is only 4 m.

Unconsolidated sand, pebbles, and cobbles are present in the upper 2 m of the northwest channel wall along fault B (Qyg in Fig. 12). These deposits are clast-supported and are not lithified like the San Timoteo Formation below them, and they do not show the oxidation and weathering of the older alluvium on the southwest side of the fault zone. Neither of the stream gravel deposits (Qyg and Qyg?) are weathered and bioturbated, as are the lower paleochannel deposits in trench 1, and although the higher exposed gravels (Qyg?) could possibly be the base of the paleochannel fill, the lower exposed gravels are in a position that is too low to be paleochannel deposits associated with the most recent stream capture event. We therefore interpret the lower Qyg deposits (and possibly the higher exposure, Qyg?) as fluvial deposits from the currently active channel that were deposited shortly after the avulsion occurred, and that are now positioned 7 m above the active channel due to continued incision. This interpretation supports the hypothesis that incision has eroded the fault-parallel segment that would have been created by slip along the active fault strand. Because of this possibility, we use these channel deposits as markers for measurement of maximum displacement (pX in Fig. 12), but also measure a maximum displacement if only the present-day geomorphology is considered (X in Fig. 12).

Displacement measurements across fault B are also complicated by the fact that the active channel bifurcates in the upstream direction at the fault. The northwestern fork has a much smaller drainage basin and shows geomorphic evidence of recent headward erosion and development, so the southeastern fork is probably the dominant upstream channel. However, we accounted for both of the upstream forks and measured the minimum displacement from the nearer channel wall, and the maximum from the farther channel wall (Fig. 12). The displacement of the northwest channel wall across fault B is a minimum of 8.8 m, a maximum of 18 m based on the current geomorphology, and a maximum of 27 m prior to the recent incision.

The southeast channel wall was not measured because it does not show any clear displacement where the fault crosses the channel, presumably because of recent erosion in the channel. Our preferred amount of displacement is between 18 m and 25 m, which lines up the Qyg deposits with the southeastern upstream fork (~18 m) and the northwestern upstream fork (~25 m). This preferred displacement is based on the approximate amount of displacement across the diagonal section of the stream, and the interpretation that recent incision has destroyed the fault-parallel section of the stream. Displacement in the range of 18–25 m is also consistent with the amount of offset of other channels along fault B in this area (Fig. 4).

Buried Channel

Trench exposures and age. Trench 6 was excavated in younger deposits at the mouth of a canyon located ~110 m to the southeast of trenches 1 and 5 (Figs. 3 and 12). The purpose of this trench was to search for evidence of the most recent ruptures in shallow stratigraphy, which was exposed in the trench walls and is presented in the next section. The northwest wall of trench 6 also exposed a buried channel that was truncated at its upstream end by fault B (Fig. 13). Trenches 7 and 8 exposed the displaced upstream continuation of this buried channel (Figs. 14 and 15). Everywhere it was exposed, we found the channel to be ~1 m deep, 1 m wide, and composed of cobbles, pebbles, and bedded sand scoured into San Timoteo Formation.

A detrital charcoal sample (6-11) collected from the buried channel deposits downstream of the faults returned an age of 300 ± 15 yr B.P. A second sample collected from the channel upstream of the faults (7-1a) returned an age of 305 ± 15 yr B.P. The calibrated age range of these samples is A.D. 1521 to A.D. 1648.

Displacement. The channel was displaced by two strands of fault B, which merge to the northwest of the trenches. Differential global positioning system (GPS) data were used to map out the trenches, edges of the buried channel, and the locations of the faults exposed in the trench walls (Fig. 16). The survey points were then used to calculate the amount of lateral displacement of the channel across the faults. Measurements were also made with a tape measure in the field. We measured lateral offsets of 4.9 m to 5.2 m on the southwest fault strand and 0.5 m to 0.7 m on the northeast fault strand, resulting in a total lateral offset of 5.4 m to 5.9 m. Vertical offset along the southwest fault strand was not determined precisely, but was on the order of a few centimeters up on the northeast side. There was no apparent vertical offset on the northeast fault strand.

Paleoseismic Data from Trenches at the Quincy Site

Two trenches at the Quincy site exposed evidence for the most recent ground-rupturing

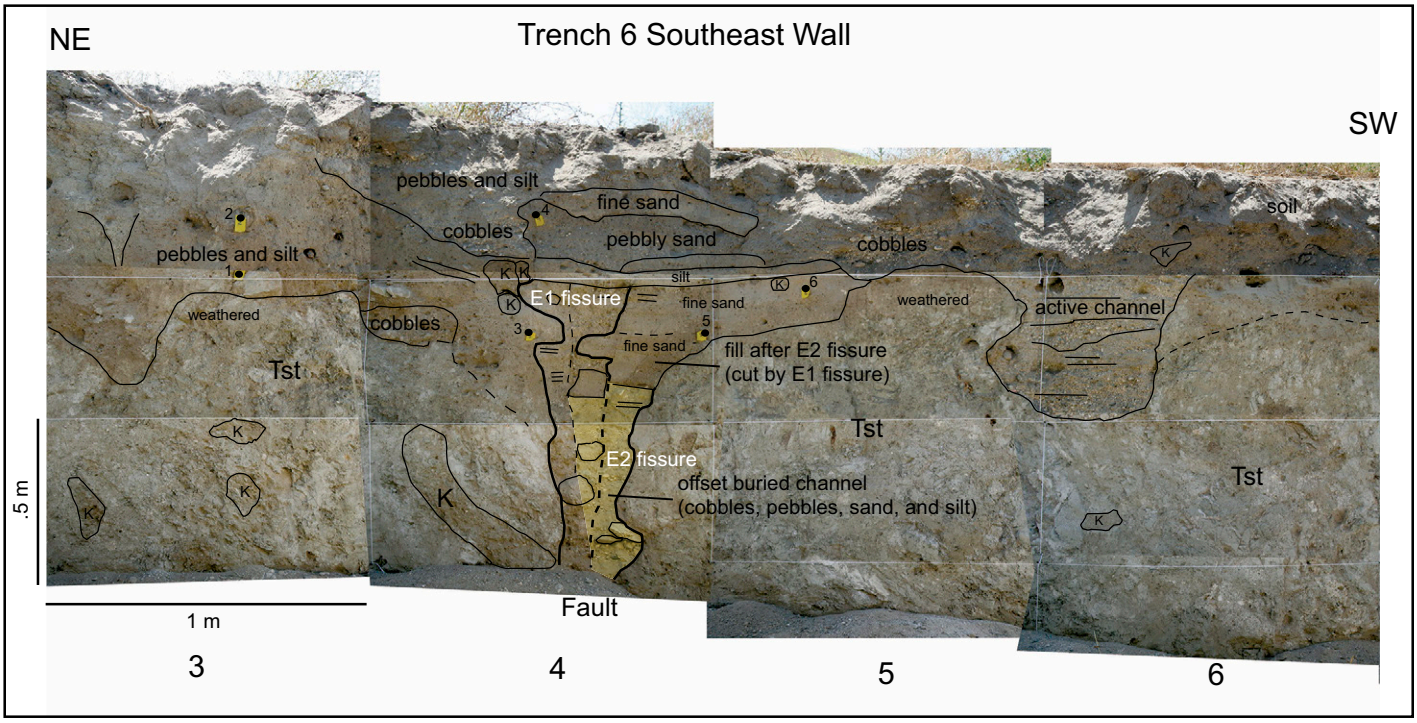

Figure 13. Photomosaic of fault B exposed in trench 6. Event 2 (E2) opened a fissure in San Timoteo Formation bedrock that was filled with sheared cobbles, gravel, and sand of the buried channel. This fissure (approximate location shown with yellow shading) was capped by later deposits, which were then faulted in event 1 (E1). Bold black lines indicate faults, and thinner black lines indicate stratigraphic contacts. Tst—Tertiary San Timoteo Formation and K—krotovina.

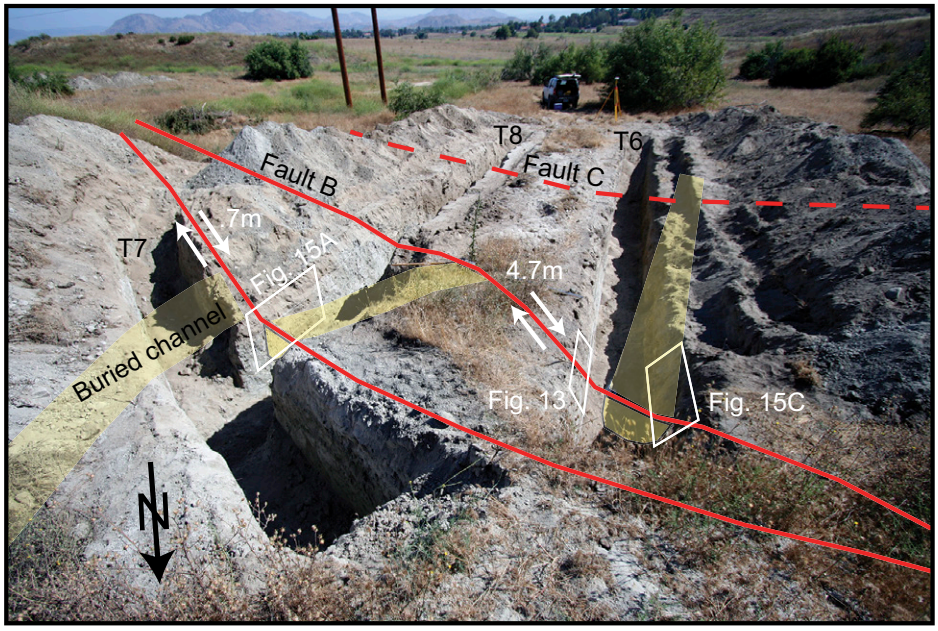

Figure 14. Photograph looking south across the fault zone at trenches 6, 7, and 8. Red lines indicate faults, the yellow shading indicates the position of the offset buried channel, and white squares indicate sections of the trench wall shown in other figures. Amounts and sense of measured displacement of the channel walls are shown in white.

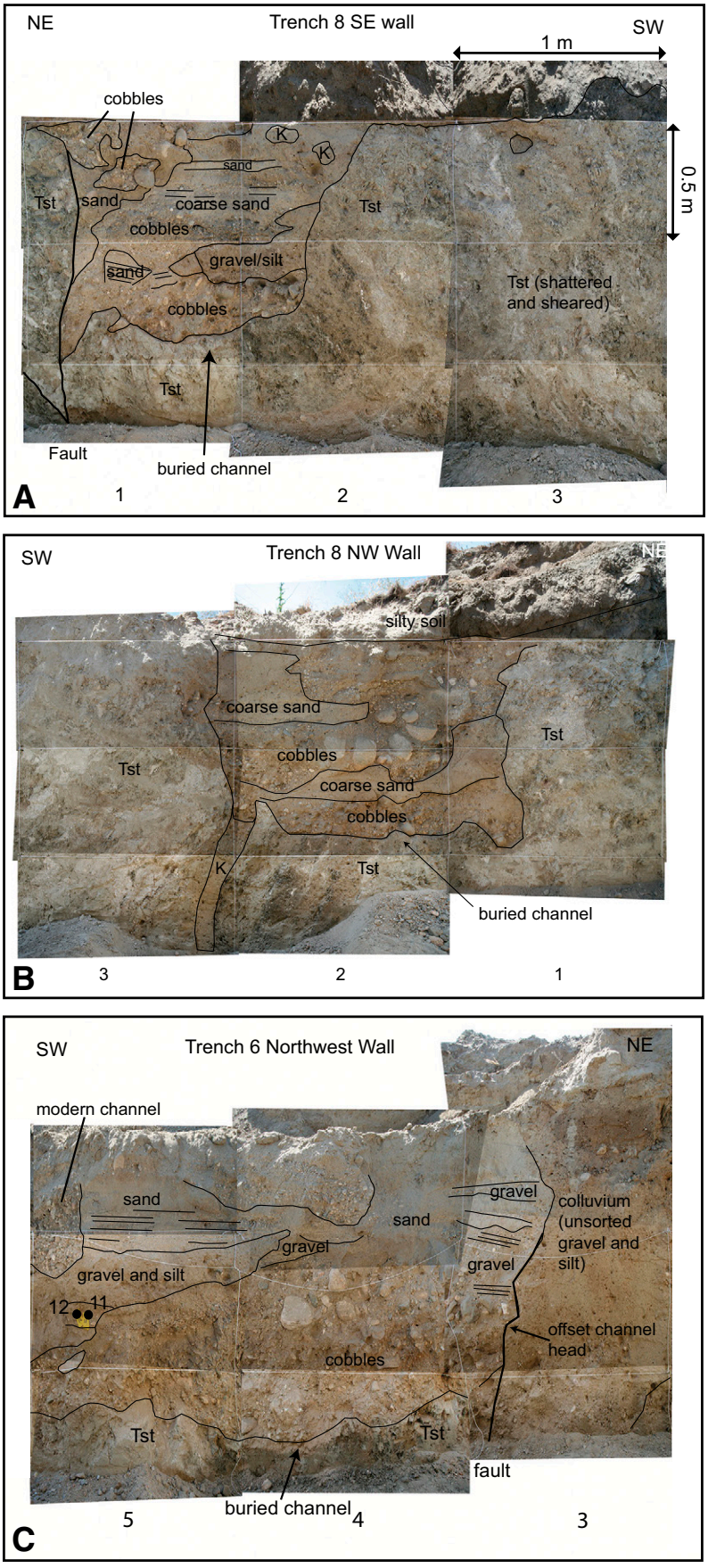

Figure 15. Photomosaics of parts of trenches 6 and 8 where the offset buried channel was exposed. (A) Exposure of the channel in the southeast wall of trench 8. The channel is developed in sheared San Timoteo Formation sedimentary rocks and is truncated on the northeast side by a fault (bold black line). (B) Exposure of the buried channel in the northwest wall of trench 8. (C) Exposure of the buried channel in the northwest wall of trench 6 (opposite to the trench panels shown in Fig. 13). Two samples used to date the offset channel are shown as black dots with label numbers. Tst—Tertiary San Timoteo Formation and K—krotovina. All three figures are the same scale and each trench panel photo is 1 m wide by 0.5 m tall.

earthquakes on the Claremont fault. The timing of the events exposed in these trenches relative to other events at the site and the event history at the Mystic Lake site is shown on Figure 11, and the details of the relationships exposed in the trenches is presented next.

Paleoseismic Data from Trench 2

Trench 2 was excavated 100 m to the northwest of trenches 1 and 5. The trench was 2 m deep and extended across both faults B and C at the margin of the badlands (Fig. 3). The trench exposures confirmed that a shutter ridge visible in older air photos was present where the stream is deflected at the mountain front. This shutter ridge, composed of San Timoteo Formation, was most likely excavated and flattened when nearby power-line poles were installed sometime after the 1940s. The stream deflection marks the location of fault B, which was seen in the trench as several small faults that offset stratigraphic units and were mainly expressed as thin fractures or zones of aligned pebbles in the coarser deposits (Fig. 17). The stratigraphy was too coarse and bioturbated to work out a precise event history, but there was strong evidence for at least two events in the upper 1.5 m of sediment. Detrital charcoal collected from the offset units returned ages of 230 ± 20 yr B.P. (Table 3), which corresponds to an OxCal calibrated age of A.D. 1643 to A.D. 1670, or A.D. 1779 to A.D. 1800. We infer that the older ages are most probable based on the fact that there have also been two events recorded at the Mystic Lake paleoseismic site since A.D. 1643, but only one since A.D. 1779 (Fig. 11; Onderdonk et al., 2013).

The trench exposures showed no evidence of rupture on fault C in the upper 2 m. Stratigraphic units exposed in the trench were continuous across the buried projection of fault C, and one detrital charcoal sample from the unfaulted deposits returned an age of 2205 ± 20 yr B.P.

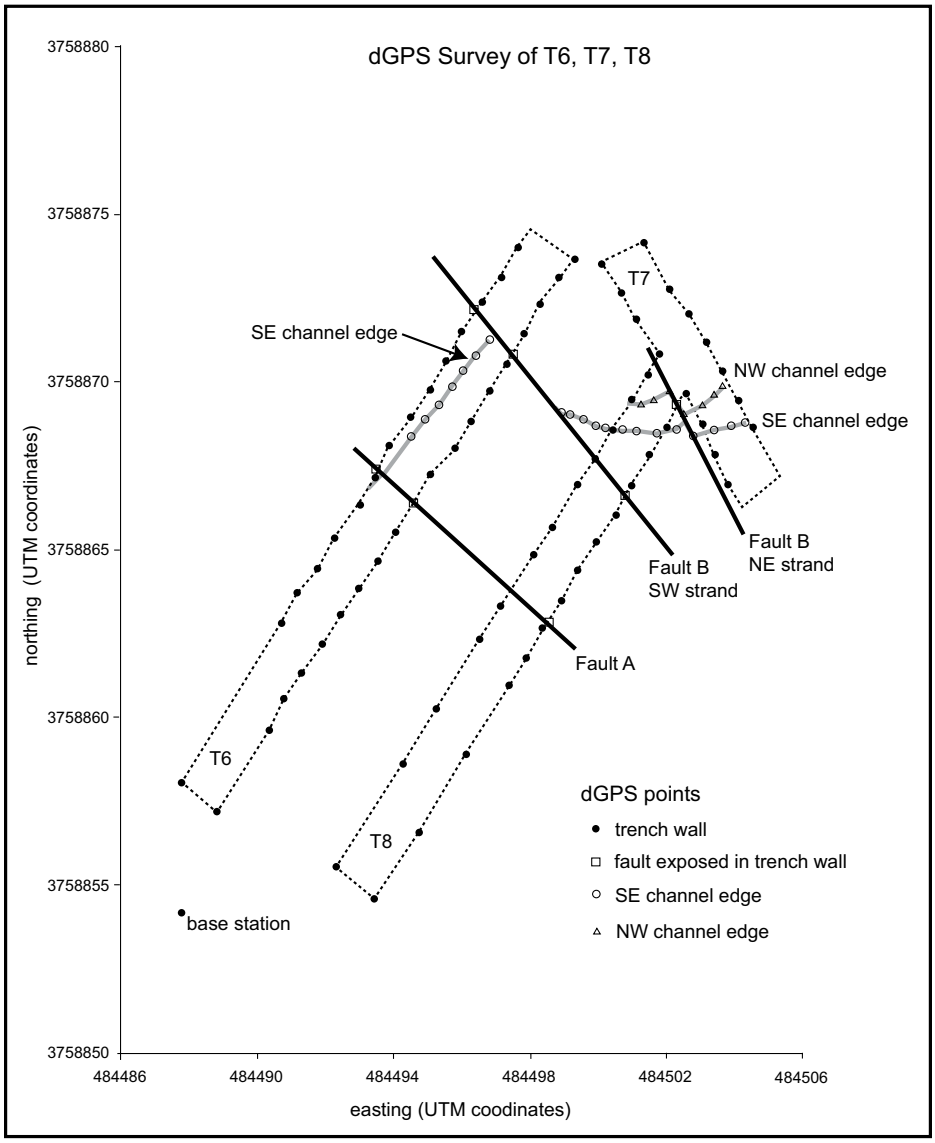

Figure 16. Map produced by differential global positioning system (dGPS) survey of trenches 6, 7, and 8. Solid dots connected by dashed lines indicate the outline of the trenches (most dots are also position on grid nails). Open squares connected by bold black lines indicate locations of faults exposed in the trench walls. Open triangles connected by gray lines indicate the northwest wall of the offset channel, and open circles connected by gray lines indicate the southeast wall.

Although the stratigraphic relationships here were not as clear as in trench 1, this supports the evidence in trench 1 that fault C has not ruptured in the past 2000 yr.

Paleoseismic Data from Trench 6

Trench 6 was ~1.5 m deep and extended across both fault B and fault C. One strand of fault B was expressed in the southeast wall of the trench as a fissure in fractured San Timoteo sandstone (Fig. 13). Two events were interpreted from the stratigraphic and faulting relationships in this exposure. The older event (E2, Fig. 13) created a fissure, which is filled with cobbles, pebbles, and bedded fine sand of the offset buried channel. These channel deposits were continuous across the floor of the trench to the exposure of the offset channel on the northwest wall of trench 6 (Fig. 15), indicating that event 2 sheared and offset the buried channel while incorporating sediment from the channel into the fissure. Fine sand was deposited on top of the channel sediments after event 2. The younger event (E1) is expressed as faults that cut the bedded fine sand layers and form a second fissure. This fissure is truncated upward by a silt layer overlain by coarser deposits related to the active channel. Detrital charcoal samples collected from this exposure were used to bracket the age of the two events. Two samples collected from the offset buried channel deposits (7-1a and 6-11) predate event 2, and two samples (6-3 and 6-6) postdate event 2 and predate event 1. The OxCal model for this fault zone (Fig. 18) constrains event 2 to be between A.D. 1530 and A.D. 1675 (with the probability density function skewed toward the younger age), and event 1 between A.D. 1680 and A.D. 1850. The upper limit of 1850 was imposed on the model based on the lack of large earthquakes that could be attributed to this fault from historic records. The ages of these events overlap with the timing of the two most recent earthquakes recorded at the Mystic Lake site (Fig. 11).

Both trench 6 and trench 8 crossed the projection of fault C. In both trenches, the upper contact of the San Timoteo Formation, which was less than a meter in depth beneath the northeastern parts of the trenches, dropped vertically below the bottom of the trenches across the projection of fault C. However, there was no evidence of faulting in the upper 1.5 m exposed in the trench walls, consistent with the evidence in trench 1 that fault C has not moved in the past 2000 yr.

INTERPRETATIONS

Slip Rate Calculations

To calculate maximum and minimum lateral slip rates, we used the amount of displacement of each feature and the amount of time over which this displacement occurred (Table 2). We determined the time range over which displacement occurred based on the timing of earthquakes on the fault. There has not been a ground-rupturing earthquake on the Claremont fault in the past 200 yr (Onderdonk et al., 2013). Consequently, using the full age of an offset feature (amount of time since the inception of the feature until today) would overestimate the time required to build up the observed offset at the surface. This is because the observed offset does not include the strain that has built up over the 200 yr since the last earthquake, which would presumably be expressed as lateral slip in the next earthquake. To account for this, we followed the approach of Sieh and Jahns (1984) and used the time between the earthquake prior to initiation of the active offset channel (or age of the buried channel) and the last (most recent) earthquake that displaced the channel, thereby capturing the time and amount of slip from complete earthquake cycles. We assumed that the earthquakes that affected the Mystic Lake site also ruptured through the Quincy site, since the two sites are only 11 km apart, and all three events recorded

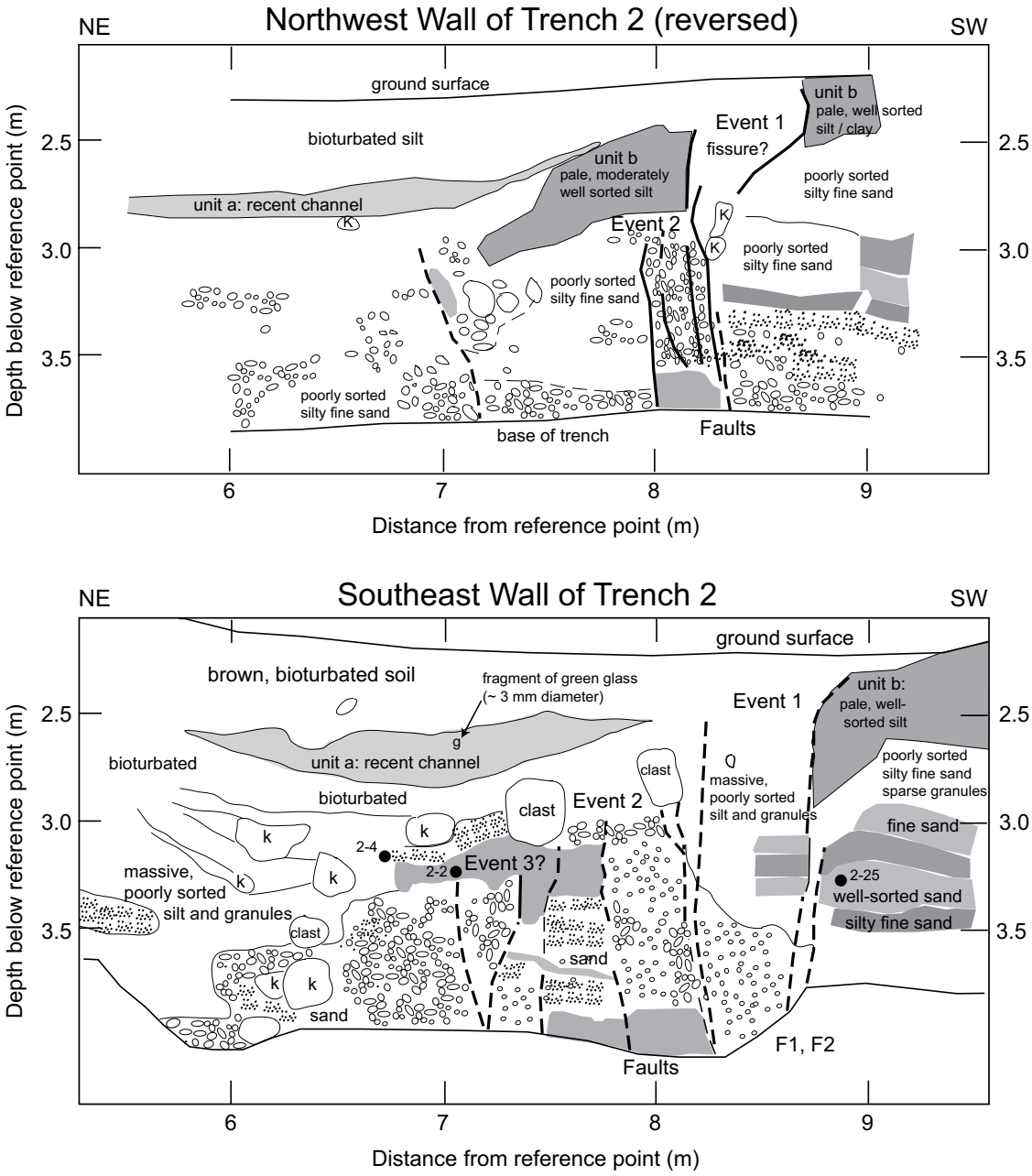

Figure 17. Trench log of both walls of trench 2 in the main fault zone of fault B. Faults are shown as thicker subvertical lines (solid and dashed). Dated detrital charcoal samples are shown as dots with numbers next to them. K—krotovina (filled animal burrow).

at the Quincy site overlap in time with events at the Mystic Lake site (E1, E2, and E12). We therefore used the timing of earthquakes at the Mystic Lake site to determine the amount of time over which the displacement of the offset features occurred.

Rates from each of the three displaced features vary depending on how many earthquake cycles are used in the calculation (see Appendix for details regarding slip rate calculations). At paleochannel 2, comparison of the age of the offset channel with the earthquake history at Mystic Lake indicates that the accumulated offset could have occurred in 9 or 10 events, and our preferred slip rates incorporate both possibilities. However, at paleochannel 1, comparison of the timing of the avulsion with the timing of events on the Claremont fault at Mystic Lake strongly favors the interpretation that displacement occurred over three earthquake cycles (Fig. 11; Appendix). This preference also holds implications for our interpretation of the number of events that have displaced the buried channel. The buried channel is displaced 4.9–5.2 m on the southwest strand of fault B, and this displacement occurred in two events based on the faulting relationships exposed in trench 6. An additional 0.5–0.7 m of displacement occurred along the northeast strand of fault B, and this could either have occurred during the same two events that ruptured the southwestern strand of fault B, or in a third, older, event. However, if the past two ruptures through the Quincy

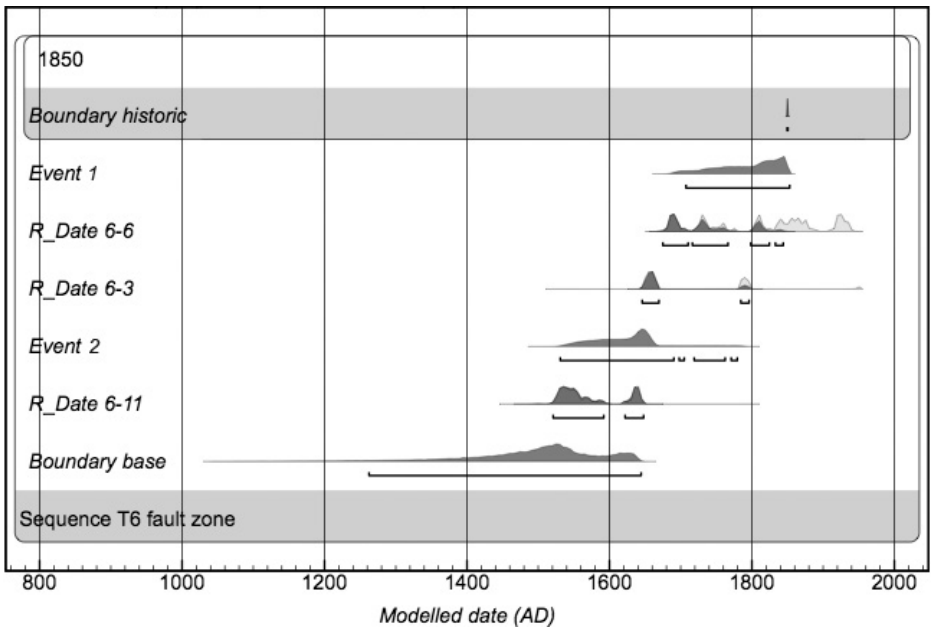

Figure 18. OxCal (Bronk Ramsey and Lee, 2013) model of the age of stratigraphic units and timing of faulting events exposed in trench T6.

site ruptured only the southwest strand of fault B and had a total of 4.9–5.2 m of displacement, this would leave at least 3.8 m of displacement that must have occurred at paleochannel 1 during the third event back in order to reach the 9 m of offset that occurred there in no more than three events. Because the buried channel is only 450 m away from paleochannel 1, we consider it very unlikely that displacement across fault B dropped from 3.8 m at paleochannel 1 to 0.7 m at the buried channel during a single rupture. Therefore, we infer that the buried channel has experienced one less earthquake than paleochannel 1, and the strongly preferred interpretation of three events displacing the active channel at paleochannel 1 implies that the buried channel was displaced in two events.

In addition to the measurements from the two paleochannels and the buried channel, a fourth calculation of slip rate can be made based on the average displacement of streams that cross fault B, along with the age of fault B inferred from relationships exposed in trench 1 and the geomorphology of the site. Fault B has displaced six of eight streams at the site by an average of 25–30 m. The two streams at the site that are not offset by this fault in a right-lateral sense are deflected in a left-lateral sense, most likely due to recent avulsion of paleochannels and capture by the current drainages. In contrast, faults A and C do not offset the presently active streams, but they have created two paleochannels, 65–110 m long, that were older channels of streams at the site (Fig. 4). Faults A and C both appear to be truncated by fault B, and fault C does not cut the younger deposits exposed in trenches 1, 2, 6, and 8, which are clearly offset by fault B. We therefore interpret that faults A and C were once continuous and have been offset 30–42 m in a right-lateral sense by slip on fault B.

Data from trenching indicate that all displacement at the Quincy site in the past ~2000 yr has occurred on fault B. Radiocarbon dates and stratigraphic relationships in trench 1 show that the last event on fault A-C occurred between 167 B.C. and A.D. 70, which overlaps in time with event 12 at Mystic Lake (Fig. 11). We infer that fault B did not move prior to the cessation of movement on fault A-C because the apparent offset of fault A-C by fault B is slightly more than the streams (by ~5–10 m; Fig. 4). This suggests that the offset streams along fault B were not offset prior to the cessation of motion along fault A-C. Using a preferred displacement amount of 25–30 m for the streams and the maximum and minimum time ranges between events 12 and 1, we calculate a slip rate of 12.8–18.3 mm/yr for the past 2050 ± 120 yr (Table 2). Absolute minimum and maximum rates are harder to determine because we are using the average offset of several streams. Nevertheless, we can estimate the minimum by assuming that the stream with the largest offset should be the oldest, and using the minimum displacement of that stream (25 m; Fig. 4) as the minimum for our calculation. Streams with less displacement may be younger and did not experience the full amount of displacement along fault B. To estimate a maximum displacement, we use the maximum displacement of fault A-C by fault B (42 m). The full range of minimum and maximum displacements yields a plausible slip rate range of 12.8–25 m/k.y. We note that the rates calculated using the displacement along, and the age of, fault B do not depend on the number of events being equal at both the Quincy and Mystic Lake sites, because they are based on the timing of earthquake ruptures documented at the Quincy site.

Calculated slip rates are listed in Table 2, and Figure 19 graphically depicts the maximum and minimum displacements and the full range of possible time over which displacement occurred for each feature, along with their preferred displacement and age ranges (shaded rectangles). Additional details regarding the slip rate calculations are presented in the Appendix.

Slip Rate Uncertainties Due to Geomorphic Interpretations

Uncertainties in the slip rate (and slip per event) calculations are partly due to uncertainties in the interpretation of the original shape and position of the offset streams at the time of stream capture. Measurements of stream displacement along a strike-slip fault typically assume that the active channel formed without a pronounced bend across the fault. However, if the active channel formed due to the upstream flow jumping into a previously developed downstream channel that had been slipping (to the northwest in this case) along the fault, the downstream channel could have been farther to the southeast or northwest and may not have been perfectly lined up with the upstream part when avulsion occurred. This means that the amount of offset could be significantly less or more than we have measured at the paleochannel locations here. There are two other places along fault B at the Quincy site where active channels are deflected in a left-lateral sense: the next active channel to the northwest of paleochannel 1 and the next active channel to the southeast of paleochannel 1 (Figs. 3 and 4). We infer that these left-lateral deflections are due to relatively recent avulsion events that caused streamflow to jump from the paleochannels at these locations to the closest downstream channel on the southwest side of the fault, which happened to be slightly to the southeast of the upstream part of the channel. If a similar situation was present for the streams we are measuring here, then we have underestimated the lateral displacement and slip rate. Conversely, if the downstream segment of the channels had already slipped past the upstream segment, we are overestimating the offset amount and slip rate. However, we con-

sider it less likely that a downstream segment would have already passed the position of an upstream segment before avulsion occurred, so we believe there is a greater chance that we have underestimated the amount of displacement and slip rate due to this source of uncertainty.

For the buried channel measurement, the displacement of the channel is well constrained by the trench exposures, and we have inferred that a change in the orientation of the channel between the two fault strands is nontectonic (Figs. 14 and 16). It is possible that this bend is due to some shear between the faults and that the actual amount of offset is greater than the maximum of 5.9 m used in our calculations.

Slip Rate Variability

The data from the Quincy site show that the slip rate of the Claremont fault varies through time when examined at shorter time scales (hundreds of years). Our longer-term slip rates from the Quincy site, calculated over 1200–2000 yr, are 12.8–18.3 mm/yr (Fig. 19). This rate is just slightly slower than the 16–20 mm/yr slip rate for the northern San Jacinto fault zone that was estimated by Morton and Matti (1993) based on an inferred fault age of 1.5 Ma and total bedrock offset along the Claremont fault of 24–30 km. Our range in slip rate is slightly faster than two previously reported slip rate calculations along the Claremont fault of 6–13 mm/yr since 50 ka (Prentice et al., 1986) and 10–16 mm/yr since ca. 100 ka (McGill et al., 2011). The overlap between our ~2000 yr rate, McGill et al.'s (2011) 100 ka rate, and Morton and Matti's (1993) 1.5 Ma rate suggests that there may be variations in slip rate of only a few millimeters per year over the lifetime of the fault. However, our short-term slip rates calculated using preferred interpretations from paleochannel 1 and the buried channel range from 21 to 30 m/k.y. (dashed lines, Fig. 19), which are ~10 mm/yr faster than the longer-term rates.

Based on data from the Quincy site and the Mystic Lake site, we interpret the recent acceleration in slip rate to be due to clustering in the timing of events in the past 600 yr and the possibility that one or more of the last few earthquakes was larger than average. The average recurrence interval for the past 2000 yr at Mystic Lake is ~164 yr (156–195 yr at 95% confidence; Onderdonk et al., 2014), whereas the recurrence times between the last four earthquakes have only been 100–140 yr (Fig. 11). The timing of events at Mystic Lake suggests a weak pattern of earthquake clustering, with the most recent cluster occurring between A.D. 1400 and A.D. 1850, preceded by a quiet period between A.D. 1000 and A.D. 1400, with a possible earlier cluster of three or more events between A.D. 640 and A.D. 1000 (events 6, 7, and 8). Sampling a slip rate during one of these clusters, as we suspect we have done at paleochannel 1 and the buried channel, would yield larger slip rates than those averaged over the past 2000 yr or more, assum-

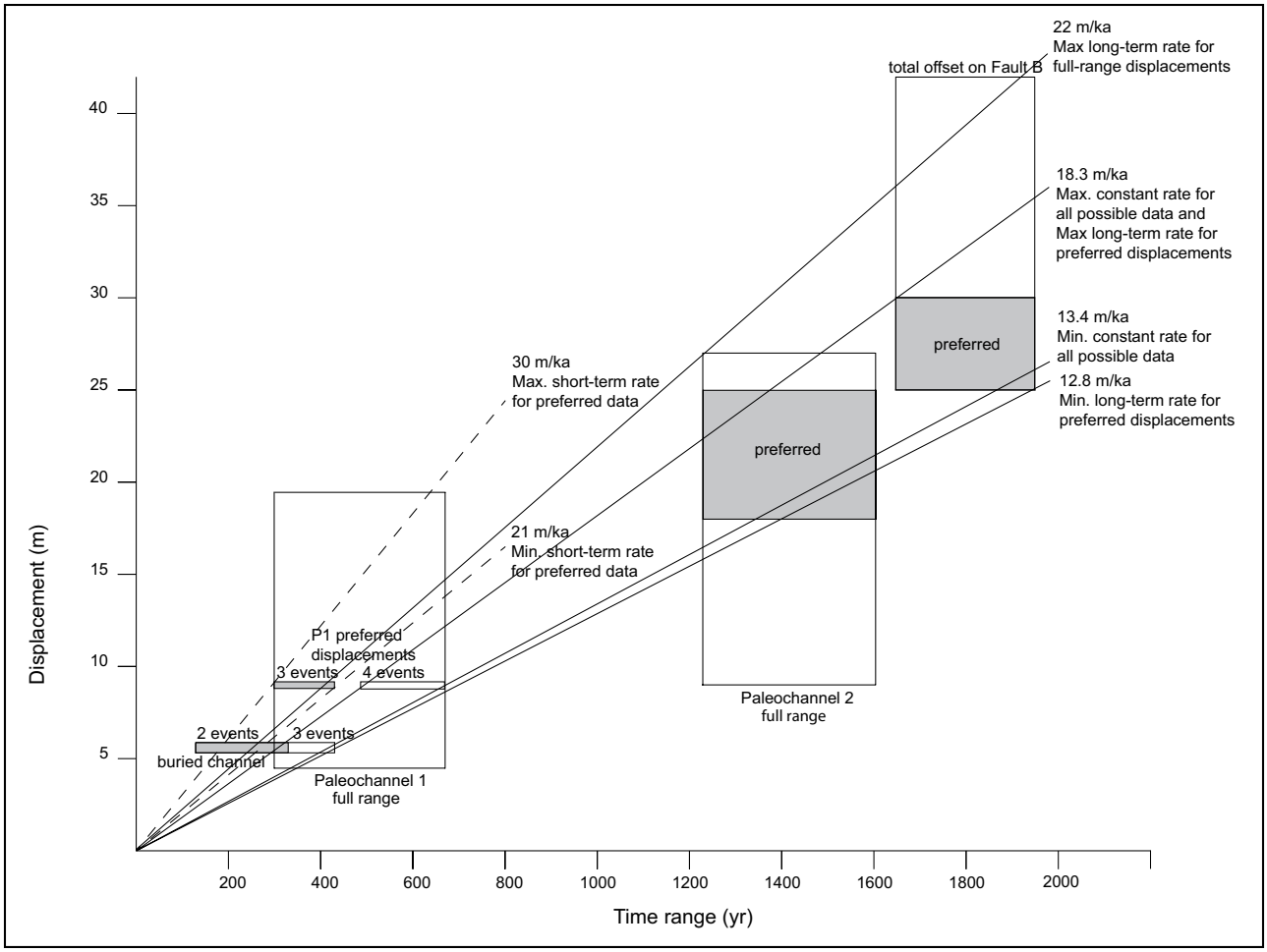

Figure 19. Plot of displacement vs. the time period over which the displacement occurred for features studied at the Quincy site. Shaded areas indicate preferred measurements. Several lines of constant slip rates are shown. "Short-term" refers to the past 500–600 yr interval, and "long-term" refers to the past 1600–2000 yr time frame.

ing slip per event is constant. If slip per event is not constant, this can also influence short-term slip rate calculations. The slip per event data at the Quincy site suggest that one or more of the last three earthquakes may have been larger than average, which would also increase the short-term slip rate. We discuss these slip per event data in a subsequent section.

Slip Rates along the Length of the San Jacinto Fault Zone

Our preferred slip rate of 12.8–18.3 mm/yr calculated at the Quincy site for the past 2000 yr considerably narrows the large range in previously reported rates from this part of the San Jacinto fault zone. The low and high ends of our preferred slip rate for the Claremont fault are ~2–3 mm/yr higher than the 10–16 mm/yr rates reported from the central San Jacinto fault to the south (Blisniuk et al., 2013; Blisniuk, 2014, personal commun.) and slightly higher than most reported geodetic rates (12–15 mm/yr). We explore three possibilities here for this difference. The first is that the true long-term slip rate for the entire San Jacinto fault zone is ~15 mm/yr, where there is agreement between our uncertainty range from the Claremont fault, the uncertainty range in Pleistocene and Holocene geologic rates from the Clark and Coyote Creek faults to the south, and the commonly reported range of geodetic rates. This rate would also satisfy the range in slip rate that McGill et al. (2013) inferred for the San Jacinto fault based on slip rate data from the San Andreas fault and nearby reverse faults of the Transverse Ranges.

A second interpretation is that the slip rate of the San Jacinto fault zone has increased slightly in the last 2000–5000 yr. Our rates are calculated from late Holocene geologic features (365–2000 yr old), whereas the youngest deposits used in previously published slip rates on the San Jacinto fault are ca. 5 ka (Blisniuk et al., 2013; Merifield et al., 1991). However, as noted already, our rates overlap with the long-term slip rate for the northern San Jacinto fault zone of 16–20 mm/yr (Morton and Matti, 1993). Blisniuk et al. (2013) also interpreted no change in slip rate over the lifetime of the Clark fault, since their rates calculated from 600 to 760 ka deposits did not differ significantly from rates calculated from 50 ka or 5 ka deposits. Consequently, we find this interpretation of a late Holocene change in rate to be less likely than the interpretation of a constant 15 ± 2 mm/yr rate for the entire fault zone.

A third interpretation for the difference in slip rate between the northern San Jacinto fault zone and the central San Jacinto fault zone is that some of the current slip on the Claremont fault may be transferred to the eastern fault segments of the fault zone. These faults parallel the Clark and Coyote Creek strands between San Jacinto Valley and the Borrego Badlands and include, from north to south, the Hot Springs fault, Thomas Mountain fault, Buck Ridge fault, and Santa Rosa fault (Fig. 1). All of these faults exhibit geomorphic evidence of Quaternary displacement in the form of scarps and/or deflected streams, but most authors have inferred that these fault segments are not as active as the principal strands to the west (e.g., Sharp, 1967; Onderdonk, 1998, 2012; Dorsey, 2002). There have been no published measurements of late Pleistocene or Holocene slip rates on any of these faults, but measurements of total lateral offset allow lifetime slip rates to be estimated. Lateral offsets are ~5 km on the Hot Springs fault (Hill, 1981), 1.3 km on the Thomas Mountain fault (Sharp, 1967), and 5.1–6.1 km along the Buck Ridge fault (Sharp, 1967). Only vertical offset has been documented along the Santa Rosa fault (Dorsey, 2002), so its lateral component is unknown and may be zero. Using an inception age of the San Jacinto fault zone of 1.5 Ma (Morton and Matti, 1993), the lifetime slip rates on these faults are 3.3 mm/yr for the Hot Springs fault, 0.9 mm/yr for the Thomas Mountain fault, and 3.4–4 mm/yr for the Buck Ridge fault. Despite the interpretation that these faults are not as active as the Clark and Coyote Creek faults (and may be older strands of the San Jacinto fault zone), there is recent seismicity along some of these faults (Onderdonk, 1998; Sanders et al., 1986). We therefore consider it possible that these fault strands have experienced some Holocene surface displacement and are accommodating some of the displacement (1–5 mm/yr) across the San Jacinto fault zone south of the Claremont fault.

Distribution of Slip between the San Jacinto and San Andreas Faults

Our new slip rate measurements suggest that slip rate on the northern San Jacinto fault is roughly equal to or slightly faster than the San Bernardino segment of the San Andreas fault. The 12.8–18.3 mm/yr slip rate on the Claremont fault calculated here is similar to the faster end of the Holocene rate of 7.0–15.7 mm/yr on the San Andreas fault (McGill et al., 2013). These ranges in slip rates determined independently for the two faults can be refined when they are evaluated in tandem. The Mojave segment of the San Andreas fault, north of the juncture between the northern San Jacinto fault and San Bernardino segment of the San Andreas fault, has a slip rate of ~35 mm/yr (Matmon et al., 2005; Humphreys and Weldon, 1994; Salyards et al., 1992). McGill et al. (2013) estimated that 5 ± 3 mm/yr of this 35 mm/yr slip could be accommodated to the south by reverse faults in the Transverse Ranges east and west of the juncture of the San Jacinto fault and the San Andreas fault, or on the Mill Creek fault of the San Andreas fault. This leaves 27–33 mm/yr that must be distributed between the northern San Jacinto fault and the San Bernardino section of the San Andreas fault. This suggests that the San Bernardino section of the San Andreas fault and the northern San Jacinto fault zone cannot both be slipping at their estimated minimum rates. If that were the case, these two faults combined would only contribute 19.8 mm/yr to the Mojave segment of the San Andreas fault. Neither can both faults be slipping at their maximum rates, for this would contribute 34 mm/yr to the Mojave segment of the San Andreas fault. If the 27–33 mm/yr slip rate is equally divided between the two faults to the south, the slip rate of each would be in the range of 13.5–16.5 mm/yr.

In a San Jacinto–dominated scenario, where we assume the northern San Jacinto fault is accommodating the maximum rate we calculated (18.3 mm/yr), and 27–33 mm/yr must be divided between the two faults, the San Bernardino section of the San Andreas slip rate would be 8.7–14.7 mm/yr. The low end of this range is slightly faster than the minimum of 7 mm/yr calculated by McGill et al. (2013).

Conversely, if we assume the San Bernardino segment of the San Andreas fault is slipping at its maximum rate (15.7 mm/yr) and subtract this from the 27–33 mm/yr that must be divided between the two faults, the slip rate for the northern San Jacinto fault is 11.3–17.5 mm/yr. The low end of this range is slower than the measured minimum at the Quincy site and hence does not refine the slip rate for the northern San Jacinto fault. This implies that the San Bernardino segment cannot be slipping at the maximum rate determined by McGill et al. (2013), or the minimum rate we have determined for the northern San Jacinto fault is too high.

Recent geodetic studies seem to favor the San Jacinto–dominated scenario when looking specifically at the northern San Jacinto fault and San Bernardino segment of the San Andreas fault (e.g., Meade and Hager, 2005; Spinler et al., 2010; Loveless and Meade, 2011; McGill et al., 2014). These studies, which use elastic models of geodetic data, consistently suggest slower slip rates on the San Bernardino segment of the San Andreas fault than along the San Andreas in Coachella Valley, most likely due to faults of the Eastern California shear zone accommodating some of the displacement north of Coachella Valley.

Our new data do not support the interpretations of Bennett et al. (2004), who tried to reconcile differences in long- and short-term slip rates by proposing a model in which slip rates on the San Jacinto fault and the southern San Andreas fault have varied inversely during the past 1.5 m.y. The interpretation that the San Jacinto fault had slip rates of 20–30 mm/yr from 1 Ma to 90 ka and then decreased to 9 ± 2mm/yr for the past 10 k.y. (Bennett et al., 2004) does not agree with our 2000 yr slip rates of 12.8–18.3 mm/yr, nor does it agree with recent work on the central San Jacinto fault, which shows little change in slip rates determined since 5 ka, 50 ka, and 600–760 ka (Blisniuk et al., 2013). The summary of slip rate calculations along the San Jacinto fault presented in the previous section seems to suggest little variability in slip rates over time scales of thousands of years or more, although we document shorter-term variations due to clustering of earthquakes through time.

Slip per Event Calculations and Variability over the Past 11 Earthquakes

Slip per event calculations were made for each of the three sites, as well as for the total offset along fault B, using the amount of offset and the number of events that offset the features. The number of events was inferred by comparing the age of the offset feature determined at the Quincy site to the timing of events on the Claremont fault recorded at the Mystic Lake site, except for the buried channel, where there was direct evidence for the number of earthquakes exposed in the trenches. Table 2 lists the "full range" of average slip per event, and the "preferred" average slip per event (in bold) for each offset feature.

As with the slip rate estimates, the average slip per event has varied during the past 2000 yr on the Claremont fault. Average slip per event for the past 9–12 events is 1.8–2.8 m, while the average slip per event for the last three events, based on preferred offset amounts and number of events, is 2.7–3 m. This change may be the result of one or more of the last three events being larger than average. An alternative, and more interesting interpretation, is that the size of ruptures on the Claremont fault may be gradually increasing over the past 2000 yr. We can evaluate this possibility by comparing the average slip per event in the last three events to the average slip per event for events 10 through 4. If we subtract the preferred 9 m of slip expressed at paleochannel 1 that accumulated during the last three events from the preferred slip amounts for paleochannel 2, which occurred during 9–10 earthquakes, we get 9–16 m of offset that must have occurred in six or seven events. This yields an average slip per event of 1.3–2.7 m for those events. Applying the same approach for events 11 through 4 using the total offset on fault B, we get an average slip per event of 2–2.6 m. Although both these ranges are slower than the average of 2.7–3 m measured over the past three events, the differences do not seem big enough to support a drastic change in slip per event through time, and a constant average slip per event of around 2.7 m is possible. We consider the possibility that one of the last three earthquakes was larger than normal to be the least complicated explanation for apparent change in slip per event over time.

Uncertainties Associated with Inferred Number of Events

For three of the four slip per event calculations, we are inferring that the number of earthquakes at the Quincy site in any given time period is the same as the Mystic Lake site. This introduces uncertainty because it is possible that some ruptures died out in between these two sites. At paleochannel 1, the slip per event of 3 m, calculated from the preferred offset amounts and the preferred interpretation of three events, is very close to the 2.7–2.95 m estimated for the last two events at the buried channel site. If we consider the less likely possibility that four events caused the 9 m of displacement at paleochannel 1, the average slip per event would be 2.25 m. It is possible that one of the last four ruptures at the Quincy site did not reach the Mystic Lake site (and the resultant slip per event is represented in Table 2), but we consider it highly unlikely that more than four events occurred at the Quincy site after the avulsion of paleochannel 1, because this would require a significant difference in recurrence interval along strike of the fault over a distance of only 11 km. At paleochannel 2, the longer time frame over which the number of events is inferred increases the chances of one or more ruptures dying out in between the Quincy and Mystic Lake sites. If we consider that two or even three ruptures may have terminated between the sites, the average slip per event could vary from less than 0.5 m to over 4 m. However, the relationships derived by Biasi and Weldon (2006), which relate slip per event at a point on a fault to earthquake size and rupture length, indicate that slip per event of 1 m or more would not die out over a distance of only 11 km. Only the average slip per event for the two most recent ruptures is based solely on data from the Quincy site. These two events can also be confidently correlated along the Claremont fault based on the similar timing of the last two events at the Quincy and Mystic Lake sites, and the fact that two events during this time were also recorded at the Colton paleoseismic site 18 km to the northwest of the Quincy site (Figs. 2 and 3; Kendrick and Fumal, 2005).

Implications of Slip per Event for Earthquake Size and Rupture across Fault Steps

The average slip per event determined here can be used to infer the average size and rupture length of ground-rupturing earthquakes on the Claremont fault and provides insight into the possibility that some earthquakes have ruptured across one of the step overs at either end of the Claremont fault. If we assume that our slip per event measurements of ~2–3 m represent average surface displacement on the fault during ruptures, this range in slip per event corresponds to earthquake magnitudes of M7.2 to M7.3 and surface rupture lengths of 75–85 km (Wells and Coppersmith, 1994). The Claremont fault is a maximum of 75 km long, so the calculated rupture lengths are equal to or slightly larger than the total fault length, suggesting that some ruptures may have continued across one of the releasing steps at the northern or southern end of the fault. Rupture patterns of 22 historic earthquakes on strike-slip faults indicate that ruptures propagated through fault steps of less than 3–4 km width ~60% of the time (Wesnousky, 2006). Both releasing steps at the ends of the Claremont fault are less than 4 km in width. At the north end of the Claremont fault, McGill et al. (2013) inferred that slip is most likely transferred between the San Andreas and San Jacinto faults within the 16 km along-strike distance between the Cajon Creek and Badger Canyon sites (Figs. 1 and 2) on the San Andreas fault, where the slip rate decreases dramatically (from ~25 to 13 mm/yr) and the parallel faults are only ~2.5 km apart. The step at the south end of the Claremont fault is no more than 4 km wide and less than 1 km wide at the north end in the vicinity of Mystic Lake (Marliyani et al., 2013). Therefore, these narrow step-over widths would not prevent ruptures from jumping across, based on the available historic data presented by Wesnousky (2006). However, 3 m of slip at the Quincy site is not large enough to confidently conclude that some ruptures continued beyond the Claremont fault because of the variability in surface displacement along ruptures, and the uncertainty in the Wells and Coppersmith (1994) relationships and those presented by Biasi and Weldon (2006).

A more robust way to evaluate the possibility that prehistoric earthquakes ruptured through a step over is to combine slip per event data for individual events with a comparison of paleoseismic data from faults on either side

of a step over. We propose that if slip per event data suggest an event ruptured a distance longer than the fault segment, and the event occurred at the same time as an event on the adjacent fault, this strongly supports an interpretation that the earthquake ruptured through the step over between the faults. At the Quincy site, a comparison of data from the buried channel and paleochannel 1 allows us to infer the amount of displacement at the site for a single event. The total displacement of 5.4–5.9 m at the buried channel site occurred in the past two or three events. If our preferred interpretation of two events is correct, we can subtract this amount from the 9 m of displacement that occurred in the last three events at paleochannel 1 and see that the third event back (event 3 at Mystic Lake; Fig. 11) had 3.1–3.6 m of displacement. The alternative interpretation of the buried channel is that the 0.5–0.7 m of displacement on the northeast strand of fault B occurred in the third event, and only the 4.9–5.2 m of displacement on the southwest strand of fault B occurred in the last two events (see Results section). In this case, there would be 3.8–4.1 m of displacement during event E3, although it is highly unlikely that ~4 m of slip at paleochannel 1 could drop to 0.7 m over a distance of 450 m. In either case, the data suggest that event E3 was larger than average, with displacement of over 3 m, which suggests a rupture length (>85 km) that is longer than the Claremont fault (75 km). Onderdonk et al. (2013, 2014) compared the timing of prehistoric earthquakes recorded at the Mystic Lake site to the timing of earthquakes at the Hog Lake site on the Clark fault (Rockwell et al., 2014) and found several possible correlations. One of these is event 3 at Mystic Lake, which occurred sometime between A.D. 1521 and A.D. 1616 coincident in time with an event recorded at Hog Lake that occurred between A.D. 1520 and A.D. 1630 (Onderdonk et al., 2013; Rockwell et al., 2014). The slip per event data that indicate event 3 was larger than average, and the paleoseismic data that indicate the occurrence of an event on the Clark fault on the other side of the step at the same time are strong evidence that event 3 ruptured through the step over at the southern end of the Claremont fault.

Overlaps in the timing of other prehistoric earthquakes recorded at the Mystic Lake site with earthquakes recorded at the Wrightwood paleoseismic site on the San Andreas fault (Fumal et al., 2002) suggest that other ruptures in the past 2000 yr may have also jumped the step over between these two faults (Onderdonk et al., 2013, 2014; Rockwell et al., 2014). If slip per event data can be obtained for these events, this would provide a way to test for coeval rupture of the San Andreas and San Jacinto faults.

CONCLUSIONS

The age and amount of offset of active streams and one buried stream channel indicate that the slip rate of the northern San Jacinto fault zone over the past 2000 yr is 12.8–18.3 mm/yr. This range overlaps with the faster end of most of the recently reported late Quaternary geologic slip rate measurements from the central San Jacinto fault zone, as well as the rates derived from geodesy. The slight difference in estimated rates between the northern and central sections of the San Jacinto fault zone (~2–3 mm/yr) may be due to uncertainties in the slip rate estimates or may indicate that some displacement on the northern San Jacinto fault zone is accommodated to the south by the Hot Springs–Thomas Mountain–Buck Ridge fault trend. Comparison of the new slip rate measurements to those along the San Bernardino segment of the San Andreas fault suggests that the slip rate on the northern San Jacinto fault is equal to or slightly higher than that along the southern San Andreas fault.

Slip rates calculated over the past two or three earthquake cycles are faster and range from 21 to 30 mm/yr. We infer that these faster short-term rates are due to a cluster of earthquakes, and/or one or more earthquakes with larger than average lateral displacement, between A.D. 1425 and A.D. 1850.

The average slip per event for the past several earthquakes is 2.7–3 m, which is slightly larger than the average slip per event of ~2.5 m for the past 11 earthquakes, and we infer this difference to be due to one or more recent larger than normal ruptures. The calculated displacement of 3.1 m or more for event 3 corresponds to rupture lengths that are slightly longer than the total length of the Claremont fault. This calculation, combined with the fact that the timing of event 3 on the Claremont fault is coeval with an event on the Clark fault recorded at the Hog Lake paleoseismic site, strongly suggests that this event ruptured through the step over between these two faults. This is the strongest geologic evidence for prehistoric rupture across step overs in the southern San Andreas fault system.

APPENDIX—CALCULATIONS OF SLIP RATE

Paleochannel 1

At Mystic Lake, three and possibly four earthquakes have occurred since the avulsion event at paleochannel 1 between A.D. 1426 and A.D. 1494 (Fig. 8; Onderdonk et al., 2013, 2014). Event 4 at Mystic Lake occurred sometime between A.D. 1422 and A.D. 1444, which overlaps with the earlier time range of the avulsion event. It is likely that avulsion at the paleochannel 1 was triggered by this earthquake, or it occurred shortly after the earthquake, since the paleochannel would have become suddenly longer due to the added slip from the earthquake. We consider it far less probable that the avulsion occurred just prior to this earthquake because the previous earthquake was at least 150 yr prior to that. An avulsion is ultimately due to a lengthening and associated decrease in slope of the fault-parallel section of an offset stream, which forces aggradation of the channel, and we assume that there is a greater chance of avulsion occurring during one of the next big storms after an offset stream is lengthened and the local geomorphology disturbed during an earthquake. Consequently, we prefer the interpretation that the active channel has experienced only three earthquakes since its initiation, although we include event 4 and the preceding time period in our slip rate calculations as an absolute minimum rate. The most recent earthquake occurred sometime between A.D. 1744 and A.D. 1850, with the upper limit imposed by the lack of any report of ground-rupturing earthquakes on the Claremont fault in historic records (Onderdonk et al., 2013).

Using the maximum possible displacement (18.9 m) with the shortest possible time period of three earthquake cycles (A.D. 1444 to A.D. 1744), we find an absolute maximum of 63 m/k.y., which is greater than the total rate of slip across the entire plate boundary and is therefore highly unlikely and would require elastic strain to have been stored across multiple earthquake cycles. The minimum possible displacement (4.5 m) divided by the longest possible time period of four earthquake cycles (A.D. 1182 to A.D. 1850) yields an absolute minimum rate of 6.7 m/k.y.

This range in slip rate can be trimmed considerably if we use our preferred displacement amount of 9 m, and the strongly preferred interpretation that the offset of the active channel occurred in three earthquakes. Using the maximum and minimum age ranges of event 1 and event 4, we calculate a preferred slip rate of 21 m/k.y. to 30 m/k.y. for the time period between A.D. 1422 and A.D. 1850 (Table 2). If we consider the less-likely chance that the avulsion occurred just prior to event 4, such that the 9 m of displacement accrued in four events, we calculate a slip rate of 13.5 m/k.y. to 18.6 m/k.y.

An alternative method of calculating the slip rate for paleochannel 1 is to drop the assumption that the number and timing of ruptures affecting the Quincy and Mystic Lake sites are the same, and simply use the time between initiation of the active channel (time of avulsion) and the present (2014), along with the amount of displacement. For the preferred displacement of 9 m, this method results in a slip rate between 15.3 m/k.y. and 17.3 m/k.y. These rates are closer to the Quaternary and Holocene slip rates measured along the San Jacinto fault zone to the south (Blisniuk et al., 2013), but they do not take into account that there has not been a surface rupture along the Claremont fault in at least the past 165 yr according to historical records (Toppazada et al., 1981), which is roughly equal to the average recurrence interval along the Claremont fault (Onderdonk et al., 2013, 2014). This lack of a surface rupture implies that the strain that has accumulated since the most recent rupture is not included in this measurement and that a surface rupture in the near future would presumably add to the offset of the channel without much change in the amount of time used in the slip rate calculation. This would elevate the resulting short-term slip rate to values equal to those calculated using our first approach.

Paleochannel 2

To calculate slip rates at paleochannel 2, we assume that the number and timing of ruptures recorded at the Mystic Lake site are the same as at the Quincy site in order to estimate the amount of time in which the measured displacement accrued. The avulsion of paleochannel 2 occurred sometime between A.D. 345 and A.D. 520, which overlaps with event 10 at Mystic Lake (Fig. 8). To calculate a minimum slip rate, we assume event 10 occurred after the avulsion and use the maximum time between event 11 and event 1 (A.D. 244 to A.D. 1850), along with the minimum displacement of the channel (8.8 m), which yields a slip rate of 5.5 m/k.y. To calculate a maximum slip rate, we assume event 10 occurred prior to the avulsion and use the minimum time between event 10 and event 1 (A.D. 514 to A.D. 1744), along with the maximum displacement of the channel (27 m), which yields a slip rate of 22 m/k.y. Using a preferred offset amount of 18–25 m, and the same minimum and maximum time frames, we calculate a slip rate of 11.3 m/k.y. to 20.3 m/k.y. over the past nine or 10 earthquake cycles (Table 2).

If the Mystic Lake event history is not applied to the Quincy site, and we calculate the slip rate based solely on the age of the active channel and the preferred displacement amount, we calculate a slip rate of between 10.8 and

16.7 m/k.y. However, as explained already, this method does not account for accumulated strain since the last earthquake, which occurred over 165 yr ago.

Buried Channel

To calculate a short-term slip rate, we consider two possibilities for the number of earthquakes that have displaced the buried channel. First, we assume that one or both of the events that occurred on the southwest strand of fault B, seen in the fault zone exposed in trench 6, also caused the smaller displacement on the northeast strand of fault B, where we do not have paleoseismic data. We use the maximum and minimum time between event 3 and event 1 at Mystic Lake, along with the total amount of offset of the channel, which yields a minimum rate of 16.4 m/k.y. and a maximum rate of 46 m/k.y. An alternative explanation is that the two earthquakes that occurred on the southwest strand of fault B did not affect the northeast strand and that displacement along the northeastern strand occurred in a third earthquake, presumably event 3 at Mystic Lake. This would mean that the buried channel was displaced in three earthquakes and gives a slip rate of 12.6 m/k.y. to 19.7 m/k.y. (Table 2).

ACKNOWLEDGMENTS

We would like to thank Gayatri Marliyani, Rebecca Tsang, Nissa Morton, Jon Guillaume, Mike Cannon, Rick Lee, and Ziad Sedki for assistance in the field and Katherine Kendrick for input and discussions in the field. We also thank Doug Yule, Mike Oskin, and Eric Kirby for excellent reviews that greatly improved this paper. This research was supported by the Southern California Earthquake Center. SCEC is funded by NSF Cooperative Agreement EAR-1033462 and USGS Cooperative Agreement G12AC20038. The SCEC contribution number for this paper is 2061.

REFERENCES CITED

Allen, M., Jackson, J., and Walker, R., 2004, Late Cenozoic reorganization of the Arabia-Eurasia collision and the comparison of short-term and long-term deformation rates: Tectonics, v. 23, p. TC2008, doi:10.1029/2003TC001530.

Atwater, T., and Stock, J., 1998, Pacific–North America plate tectonics of the Neogene Southwestern United States: An update: International Geology Review, v. 40, no. 5, p. 375–402, doi:10.1080/00206819809465216.

Becker, T.W., Hardebeck, J.L., and Anderson, G., 2005, Constraints on fault slip rates of the southern California plate boundary from GPS velocity and stress inversions: Geophysical Journal International, v. 160, p. 634–650, doi: 10.1111/j.1365-246X.2004.02528.x.

Behr, W.M., Rood, D.H., Fletcher, K.E., Guzman, N., Finkel, R., Hanks, T.C., Hudnut, K.W., Kendrick, K.J., Platt, J.P., and Sharp, W.D., 2010, Uncertainties in slip-rate estimates for the Mission Creek strand of the southern San Andreas fault at Biskra Palms Oasis, southern California: Geological Society of America Bulletin, v. 122, p. 1360–1377, doi:10.1130/B30020.1.

Bennett, R.A., Friedrich, A.M., and Furlong, K.P., 2004, Codependent histories of the San Andreas and San Jacinto fault zones from inversion of fault displacement rates: Geology, v. 32, no. 11, p. 961–964, doi:10.1130/G20806.1.

Bevis, M., Hudnut, K., Brzezinska, D., Sanchez, R., and Toth, C., 2006, The B4 LiDAR survey of the southern San Andreas and San Jacinto faults: Seismological Research Letters, v. 77, p. 311.

Biasi, G.P., and Weldon, R.J., 2006, Estimating surface rupture length and magnitude of paleoearthquakes from point measurements of rupture displacement: Bulletin of the Seismological Society of America, v. 96, no. 5, p. 1612–1623, doi:10.1785/0120040172.

Blisniuk, K., Rockwell, T., Owen, L.A., Oskin, M., Lippincott, C., Caffee, M.W., and Dortch, J., 2010, Late Quaternary slip rate gradient defined using high-resolution topography and ^{10}Be dating of offset landforms on the southern San Jacinto fault zone, California: Journal of Geophysical Research, v. 115, p. B08401, doi:10.1029/2009JB006346.

Blisniuk, K., Oskin, M., Mériaux, A.-S., Rockwell, T., Finkel, R.C., and Ryerson, F.J., 2013, Stable, rapid rate of slip since inception of the San Jacinto fault, California: Quaternary San Jacinto fault slip rates: Geophysical Research Letters, v. 40, p. 4209–4213, doi:10.1002/grl.50819.

Bronk Ramsey, C., 2009, Bayesian analysis of radiocarbon dates: Radiocarbon, v. 51, p. 337–360.

Bronk Ramsey, C., and Lee, S., 2013, Recent and planned developments of the program OxCal: Radiocarbon, v. 55, p. 3–4, doi:10.2458/azu_js_rc.55.16215.

DeMets, C., and Dixon, T.H., 1999, New kinematic models for Pacific–North America motion from 3 Ma to present: I. Evidence for steady motion and biases in the Nuvel-1A model: Geophysical Research Letters, v. 26, p. 1921–1924, doi:10.1029/1999GL900405.

Dolan, J.F., Bowman, D.B., and Sammis, C.G., 2007, Long-range and long-term fault interactions in Southern California: Geology, v. 35, no. 9, p. 855–858, doi:10.1130/G23789A.1.

Dorsey, R.J., 2002, Stratigraphic record of Pleistocene initiation and slip on the Coyote Creek fault, lower Coyote Creek, southern California, *in* Barth, A., ed., Contributions to Crustal Evolution of the Southwestern United States: Geological Society of America Special Paper 365, p. 251–269.

Fay, N.P., and Humphreys, E.D., 2005, Fault slip rates, effects of elastic heterogeneity on geodetic data, and the strength of the lower crust in the Salton Trough region, southern California: Journal of Geophysical Research, v. 110, p. B09401, doi:10.1029/2004JB003548.

Fumal, T.E., Weldon, R.J., Biasi, G.P., Dawson, T.E., Seitz, G.G., Frost, W.T., and Schwartz, D.P., 2002, Evidence for large earthquakes on the San Andreas fault at the Wrightwood, California, paleoseismic site: A.D. 500 to present: Bulletin of the Seismological Society of America, v. 92, p. 2726–2760, doi:10.1785/0120000608.

Harden, J.W., and Matti, J.C., 1989, Holocene and late Pleistocene slip rates on the San Andreas fault in Yucaipa, California, using displaced alluvial-fan deposits and soil chronology: Geological Society of America Bulletin, v. 101, p. 1107–1117, doi:10.1130/0016-7606(1989)101<1107:HALPSR>2.3.CO;2.

Hill, R.I., 1981, Field, petrologic, and isotopic studies of the intrusive complex of San Jacinto Mountain, *in* Brown, A.R., and Ruff, R.W., eds., Geology of the San Jacinto Mountains: Santa Ana, California, South Coast Geological Society, Annual Field Trip Guidebook 9, p. 76–89.

Humphreys, E.D., and Weldon, R.J., 1994, Deformation across the western United States: A local estimate of Pacific–North America transform deformation: Journal of Geophysical Research, v. 99, no. B10, p. 19,975–20,010, doi:10.1029/94JB00899.

Janecke, S.U., Dorsey, R.J., Forand, D., Steely, A.N., Kirby, S.M., Lutz, A.T., Housen, B.A., Belgarde, B., Langenheim, V.E., and Rittenour, T.M., 2011, High Geologic Slip Rates since Early Pleistocene Initiation of the San Jacinto and San Felipe Fault Zones in the San Andreas Fault System: Southern California, USA: Geological Society of America Special Paper 475, 48 p., doi:10.1130/2010.2475.

Kendrick, K.J., and Fumal, T., 2005, Paleoseismicity of the northern San Jacinto fault, Colton and San Bernardino, Southern California; preliminary results: Geological Society of America Abstracts with Programs, v. 37, no. 7, p. 559.

Kendrick, K.J., Morton, D.M., Wells, S.G., and Simpson, R.W., 2002, Spatial and temporal deformation along the northern San Jacinto fault, Southern California: Implications for slip rates: Bulletin of the Seismological Society of America, v. 92, no. 7, p. 2782–2802, doi:10.1785/0120000615.

Loveless, J.P., and Meade, B.J., 2011, Stress modulation on the San Andreas fault by interseismic fault system interactions: Geology, v. 39, p. 1035–1038, doi:10.1130/G32215.1.

Marliyani, G.I., Rockwell, T.K., Onderdonk, N.W., and McGill, S.F., 2013, Straightening of the northern San Jacinto fault, California, as seen in the fault-structure evolution of the San Jacinto stepover: Bulletin of the Seismological Society of America, v. 103, no. 3, p. 2047–2061, doi: 10.1785/0120120232.

Matmon, A., Schwartz, D.P., Finkel, R., Clemmens, S., and Hanks, T., 2005, Dating offset fans along the Mojave section of the San Andreas fault using cosmogenic ^{26}Al and ^{10}Be: Geological Society of America Bulletin, v. 117, p. 795–807, doi:10.1130/B25590.1.

McGill, S., Dergham, S., Barton, K., Berney-Ficklin, T., Grant, D., Hartling, C., Hobart, K., Minnich, R., Rodriguez, M., Runnerstrom, E., Russell, J., Schmoker, K., Stumfall, M., Townsend, J., and Williams, J., 2002, Paleoseismology of the San Andreas fault at Plunge Creek, near San Bernardino, Southern California: Bulletin of the Seismological Society of America, v. 92, p. 2803–2840, doi:10.1785/0120000607.

McGill, S., Weldon R., and Owen, L., 2010, Latest Pleistocene slip rates along the San Bernardino strand of the San Andreas fault: Geological Society of America Abstracts with Programs, v. 42, no. 4, p. 69, paper 21-4.

McGill, S.F., Owen, L.A., Kent, E.O., Rockwell, T.K., and Onderdonk, N.W., 2011, Slip rate of the northern San Jacinto fault from offset landslides in the San Timoteo Badlands: Proceedings and Abstracts, Volume XX: Palm Springs, California, Southern California Earthquake Center, Annual Meeting, 11–14 September 2011, http://www.scec.org/meetings/2011am/.

McGill, S.F., Owen, L.A., Weldon, R.J., and Kendrick, K.J., 2013, Latest Pleistocene and Holocene slip rate for the San Bernardino strand of the San Andreas fault, Plunge Creek, Southern California: Implications for strain partitioning within the southern San Andreas fault system for the last 35 k.y.: Geological Society of America Bulletin, v. 125, p. 48–72, doi:10.1130/B30647.1.

McGill, S., Spinler, J., McGill, J., Bennett, R., Floyd, M., Fryxell, J., and Funning, G., 2014, One-dimensional modeling of fault slip rates using new geodetic velocities from a transect across the Pacific–North America plate boundary through the San Bernardino Mountains, California: Proceedings and Abstracts, Volume XX: Palm Springs, California, Southern California Earthquake Center, Annual Meeting, 7–10 September 2014, http://www.scec.org/meetings/2014am/.

Meade, B.J., and Hager, B., 2005, Block models of crustal motion in southern California constrained by GPS measurements: Journal of Geophysical Research, v. 110, p. B03403, doi:10.1029/2004JB003209.

Merifield, P.M., Rockwell, T.K., and Loughman, C.C., 1991, A slip rate based on trenching studies, San Jacinto fault zone near Anza, California: Geotechnical Engineering and Engineering Geology, v. 27, p. 28:1–28:21.

Morton, D.M., and Matti, J.C., 1993, Extension and contraction within an evolving divergent strike-slip fault complex; the San Andreas and San Jacinto fault zones at their convergence in Southern California, *in* Powell, R.E., Weldon, R.J., and Matti, J.C. eds., The San Andreas Fault System: Displacement, Palinspastic Reconstruction, and Geologic Evolution: Geological Society of America Memoir 178, p. 217–230.

Onderdonk, N.W., 1998, The Tectonic Structure of the Hot Springs Fault Zone, Riverside County, California [M.S. thesis]: Santa Barbara, California, University of California Santa Barbara, 65 p.

Onderdonk, N.W., 2012, The role of the Hot Springs fault in the development of the San Jacinto fault zone and uplift of the San Jacinto Mountains, *in* Snyder, S., Miller-Hicks, B., and Miller, J., eds., Palms to Pines: Geological and Historical Excursions through the Palm Springs Region, Riverside County, California: San Diego Association of Geologists and South Coast Geological Society Field Trip Guidebook 39, p. 95–107.

Onderdonk, N.W., Rockwell, T.K., McGill, S.F., and Marliyani, G.I., 2013, Evidence for seven surface ruptures in the past 1600 years on the Claremont fault at Mystic Lake, northern San Jacinto fault zone, California: Bulletin of the Seismological Society of America, v. 103, p. 519–541, doi:10.1785/0120120060.

Onderdonk, N.W., McGill, S.F., and Rockwell, T.K., 2014, Paleoseismology of the northern San Jacinto fault zone and implications for rupture across steps in the San Andreas fault system, southern California: Seismological Research Letters, v. 85, no. 2, p. 455.

Orozco, A., 2004, Offset of a Mid-Holocene Alluvial Fan near Banning, CA; Constraints on the Slip Rate of the San Bernardino Strand of the San Andreas Fault [M.S. thesis]: Northridge, California, California State University at Northridge, 56 p.

Prentice, C.S., Weldon, R.J., and Sieh, K., 1986, Distribution of slip between the San Andreas and San Jacinto faults near San Bernardino, Southern California: Geological Society of America Abstracts with Programs, v. 18, no. 2, p. 172.

Reimer, P.J., Bard, E., Bayliss, A., Beck, J.W., Blackwell, P.G., Bronk Ramsey, C., Grootes, P.M., Guilderson, T.P., Haflidason, H., Hajdas, I., Hatté, C., Heaton, T.J., Hoffmann,

D.L., Hogg, A.G., Hughen, K.A., Kaiser, K.F., Kromer, B., Manning, S.W., Niu, M., Reimer, R.W., Richards, D.A., Scott, E.M., Southon, J.R., Staff, R.A., Turney, C.S.M., and van der Plicht, J., 2013, IntCal13 and Marine13 radiocarbon age calibration curves 0–50,000 years cal BP: Radiocarbon, v. 55, no. 4, p. 1869–1887, doi:10.2458/azu_js_rc.55.16947.

Rockwell, T., Loughman, C., and Merifield, P., 1990, Late Quaternary rate of slip along the San Jacinto fault zone near Anza, southern California: Journal of Geophysical Research, v. 95, p. 8593, doi:10.1029/JB095iB06p08593.

Rockwell, T., Dawson, T., Ben-Horin, J.Y., and Seitz, G., 2014, A 21 event, 4,000-year history of surface ruptures in the Anza seismic gap, San Jacinto fault: Implications for long-term earthquake production on a major plate boundary fault: Pure and Applied Geophysics, v. 171, no. 11, p. 2955–2965, doi:10.1007/s00024-014-0955-z.

Salyards, S.L., Sieh, K.E., and Kirschvink, J.L., 1992, Paleomagnetic measurement of nonbrittle coseismic deformation across the San Andreas fault at Pallett Creek: Journal of Geophysical Research–Solid Earth (1978–2012), v. 97, p. 12,457–12,470.

Sanders, C., Magistrale, H., and Kanamori, H., 1986, Rupture patterns and preshocks of large earthquakes in the southern San Jacinto fault zone: Bulletin of the Seismological Society of America, v. 76, p. 1187–1206.

Sarna-Wojcicki, A.M., Pringle, M.S., and Wijbrans, J., 2000, New $^{40}Ar/^{39}Ar$ age of the Bishop Tuff from multiple sites and sediment rate calibration for the Matuyama-Brunhes boundary: Journal of Geophysical Research, v. 105, p. 21,431–21,443, doi:10.1029/2000JB900901.

Sharp, R.V., 1967, San Jacinto fault zone in the Peninsular Ranges of Southern California: Geological Society of America Bulletin, v. 78, p. 705, doi:10.1130/0016-7606(1967)78[705:SJFZIT]2.0.CO;2.

Sharp, R.V., 1981, Variable rates of late Quaternary strike slip on the San Jacinto fault zone, southern California: Journal of Geophysical Research, v. 86, p. 1754, doi:10.1029/JB086iB03p01754.

Sieh, J.E., and Jahns, R.H., 1984, Holocene activity of the San Andreas fault at Wallace Creek, California: Geological Society of America Bulletin, v. 95, p. 883–896, doi:10.1130/0016-7606(1984)95<883:HAOTSA>2.0.CO;2.

Spinler, J.C., Bennett, R.A., Anderson, M.L., McGill, S.F., Hreinsdóttir, S., and McCallister, A., 2010, Present-day strain accumulation and slip rates associated with southern San Andreas and Eastern California shear zone faults: Journal of Geophysical Research, v. 115, p. B11407, doi:10.1029/2010JB007424.

Toppazada, T., Real, C., and Parke, D., 1981, Preparation of Isoseismal Maps and Summaries of Reported Effects for Pre-1900 California Earthquakes: California Division of Mines and Geology Open-File Report 81-11 SAC, 182 p.

Weldon, R.J., and Sieh, K.E., 1985, Holocene rate of slip and tentative recurrence interval for large earthquakes on the San Andreas fault, Cajon Pass, southern California: Geological Society of America Bulletin, v. 96, p. 793–812, doi:10.1130/0016-7606(1985)96<793:HROSAT>2.0.CO;2.

Wells, D.L., and Coppersmith, K.J., 1994, New empirical relationships among magnitude, rupture length, rupture width, rupture area, and surface displacement: Bulletin of the Seismological Society of America, v. 84, p. 974–1002.

Wesnousky, S.G., 2006, Predicting the endpoints of earthquake ruptures: Nature, v. 444, p. 358–360, doi:10.1038/nature05275.

Wesnousky, S.G., Prentice, C.S., and Sieh, K.E., 1991, An offset Holocene stream channel and the rate of slip along the northern reach of the San Jacinto fault zone, San Bernardino Valley, California: Geological Society of America Bulletin, v. 103, p. 700–709, doi:10.1130/0016-7606(1991)103<0700:AOHSCA>2.3.CO;2.

Yule, D., 2009, The enigmatic San Gorgonio Pass: Geology, v. 37, p. 191–192, doi:10.1130/focus022009.1.

Yule, D., and Spotila, J., 2010, Quaternary geology of the San Bernardino Mountains and their tectonic margins, *in* Clifton, E.H., and Ingersoll, R.V., eds., Geologic Excursions in California and Nevada: Tectonics, Stratigraphy and Hydrogeology: Upland, California, Pacific Section, SEPM (Society for Sedimentary Geology), Book 108, p. 273–322.

MANUSCRIPT RECEIVED 16 MAY 2014
REVISED MANUSCRIPT RECEIVED 26 NOVEMBER 2014
MANUSCRIPT ACCEPTED 21 JANUARY 2015

Printed in the USA